RESEARCH ARTICLE
Molecular Biology and Physiology

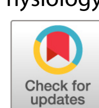

The Two-Component System CopRS Maintains Subfemtomolar Levels of Free Copper in the Periplasm of *Pseudomonas aeruginosa* Using a Phosphatase-Based Mechanism

Lorena Novoa-Aponte,[a] Cheng Xu,[a] Fernando C. Soncini,[b] José M. Argüello[a]

[a]Department of Chemistry and Biochemistry, Worcester Polytechnic Institute, Worcester, Massachusetts, USA
[b]Instituto de Biología Molecular y Celular de Rosario, Universidad Nacional de Rosario, Consejo Nacional de Investigaciones Científicas y Técnicas, Rosario, Santa Fe, Argentina

Downloaded from http://msphere.asm.org/ on December 23, 2020 by guest

ABSTRACT Two-component systems control periplasmic Cu^+ homeostasis in Gram-negative bacteria. In characterized systems such as *Escherichia coli* CusRS, upon Cu^+ binding to the periplasmic sensing region of CusS, a cytoplasmic phosphotransfer domain of the sensor phosphorylates the response regulator CusR. This drives the expression of efflux transporters, chaperones, and redox enzymes to ameliorate metal toxic effects. Here, we show that the *Pseudomonas aeruginosa* two-component sensor histidine kinase CopS exhibits a Cu-dependent phosphatase activity that maintains CopR in a nonphosphorylated state when the periplasmic Cu levels are below the activation threshold of CopS. Upon Cu^+ binding to the sensor, the phosphatase activity is blocked and the phosphorylated CopR activates transcription of the CopRS regulon. Supporting the model, mutagenesis experiments revealed that the Δ*copS* strain exhibits maximal expression of the CopRS regulon, lower intracellular Cu^+ levels, and increased Cu tolerance compared to wild-type cells. The invariant phosphoacceptor residue His_{235} of CopS was not required for the phosphatase activity itself but was necessary for its Cu dependency. To sense the metal, the periplasmic domain of CopS binds two Cu^+ ions at its dimeric interface. Homology modeling of CopS based on CusS structure (four Ag^+ binding sites) clearly supports the different binding stoichiometries in the two systems. Interestingly, CopS binds $Cu^{+/2+}$ with 3×10^{-14} M affinity, pointing to the absence of free (hydrated) $Cu^{+/2+}$ in the periplasm.

IMPORTANCE Copper is a micronutrient required as cofactor in redox enzymes. When free, copper is toxic, mismetallating proteins and generating damaging free radicals. Consequently, copper overload is a strategy that eukaryotic cells use to combat pathogens. Bacteria have developed copper-sensing transcription factors to control copper homeostasis. The cell envelope is the first compartment that has to cope with copper stress. Dedicated two-component systems control the periplasmic response to metal overload. This paper shows that the sensor kinase of the copper-sensing two-component system present in *Pseudomonadales* exhibits a signal-dependent phosphatase activity controlling the activation of its cognate response regulator, distinct from previously described periplasmic Cu sensors. Importantly, the data show that the system is activated by copper levels compatible with the absence of free copper in the cell periplasm. These observations emphasize the diversity of molecular mechanisms that have evolved in bacteria to manage the copper cellular distribution.

KEYWORDS *Pseudomonas aeruginosa*, copper, homeostasis, periplasm, two-component regulatory systems

Citation Novoa-Aponte L, Xu C, Soncini FC, Argüello JM. 2020. The two-component system CopRS maintains subfemtomolar levels of free copper in the periplasm of *Pseudomonas aeruginosa* using a phosphatase-based mechanism. mSphere 5:e01193-20. https://doi.org/10.1128/mSphere.01193-20.

Editor Craig D. Ellermeier, University of Iowa

Copyright © 2020 Novoa-Aponte et al. This is an open-access article distributed under the terms of the Creative Commons Attribution 4.0 International license.

Address correspondence to José M. Argüello, arguello@wpi.edu.

Received 24 November 2020
Accepted 27 November 2020
Published 23 December 2020

Copper is a cellular micronutrient required for redox enzymatic functions (1, 2). However, free Cu undergoes deleterious Fenton reactions, metallates noncognate binding sites, and promotes disassembly of Fe-S centers (3, 4). Early studies in the field

took advantage of Cu toxicity to identify widely distributed proteins conferring metal tolerance, namely, metal-sensing transcriptional regulators and efflux transporters (1, 4–7). Recent studies have, however, started to uncover regulated distribution systems that move the metal among cellular compartments and target Cu^+ to cognate metalloproteins while maintaining the required homeostasis (8–15). These include Cu^+-sensing transcriptional regulators, influx and efflux transmembrane transporters, chaperones, and storage molecules. In this context, bacterial cells prevent Cu toxicity by expressing some of these molecules in response to high intracellular metal conditions. The cytoplasmic response to Cu^+ excess has been characterized in numerous Gram-positive and Gram-negative bacteria (11, 16–19). Nevertheless, periplasmic components involved in Cu^+ homeostasis have received much less attention. A simple consideration of the Gram-negative bacterium architecture points out that periplasmic dyshomeostasis is likely to precede the cytoplasmic response to a surge of Cu^+ influx. Supporting this idea, mathematical simulations based on Cu^+ uptake experiments in *Pseudomonas aeruginosa* under dyshomeostasis conditions suggest that the periplasmic Cu^+ overload precedes the cytoplasmic imbalance (10). Moreover, periplasmic storage molecules are likely crucial for maintaining cellular Cu^+ allocation (10).

Cytoplasmic Cu^+-sensing transcriptional regulators are diverse, as different bacterial species have solved Cu^+ homeostasis using alternative strategies (1, 5, 20, 21). However, the periplasmic response appears usually regulated by similar two-component systems (TCSs) (22, 23). Although absent in *Salmonella* (6), many *Enterobacteriaceae* (e.g., *Escherichia coli*, *Klebsiella pneumoniae*, etc.) modulate periplasmic Cu^+ stress responses via the chromosomally encoded TCS CusRS and the plasmid-borne PcoRS (24–30). Instead, CopRS monitors extracytoplasmic Cu^+ accumulation in *Corynebacterium glutamicum* and *Synechocystis* (31–33). CopRS is also found in *Pseudomonadaceae*, including *Pseudomonas syringae* (34, 35), *P. aeruginosa* (9), and *Pseudomonas fluorescens* (36, 37).

Most TCSs comprise a sensor histidine kinase (SHK) and its cognate cytoplasmic response regulator (RR). The SHK is usually a homodimeric membrane receptor with a periplasmic sensor domain flanked by two transmembrane segments (see Fig. S1 in the supplemental material). The C-terminal cytoplasmic domain contains the catalytic machinery (38). SHKs are bifunctional enzymes that switch between kinase and phosphatase states in a signal-dependent manner. In the kinase mode, the SHK undergoes autophosphorylation of a conserved His residue and subsequently transfers the phosphoryl group to a conserved Asp residue of its cognate RR. Although some RRs have alternative roles in their unphosphorylated states (39), phosphorylation of most of the RRs allosterically modifies their transcriptional activity (Fig. 1A). TCS sensors might also operate in a phosphatase mode. In these cases, the dephosphorylated SHK catalyzes the dephosphorylation of RR (RR~P) that has been phosphorylated, metabolically or by an alternative kinase, in response to an environmental stimulus (39–43).

Ultimately, the signal-dependent balance between SHK kinase and phosphatase activities determines the RR~P levels, modulating the output response (38). In the archetypical *E. coli* CusRS TCS, Cu^+ binding to the periplasmic loop of CusS promotes its autophosphorylation and the subsequent phosphorylation of the transcriptional regulator CusR (Fig. 1A). A positive regulation has then been assumed for TCS controlling periplasmic Cu^+. Supporting this model, deletion of either the SHK CusS or the RR CusR leads to a reduced tolerance to external Cu^{2+}, increased intracellular Cu^+, and lack of transcriptional activation of regulated genes (e.g., *cusC*) (24–27).

The regulons controlled by the canonical Cu^+-responsive TCS are limited to gene systems coding for the RNDs CusCFBA (26), PcoABCDRSE (27), and CopABCDRS (34, 35). However, Cu^+ homeostatic pathways do not behave as evolutionary units. Instead, distinct species assemble different repertoires of metal handling proteins to achieve periplasmic Cu^+ homeostasis (21). In particular, the *P. aeruginosa* CopRS regulon includes genes coding for an outer membrane transporter (PcoB), a multicopper oxidase (PcoA), and auxiliary proteins (PtrA, PA2807, and QueF) whose role in periplasmic Cu^+ distribution is still unclear (44–46) (Fig. 1B). Interesting, the *P. aeruginosa* CusCBA

Downloaded from http://msphere.asm.org/ on December 23, 2020 by guest

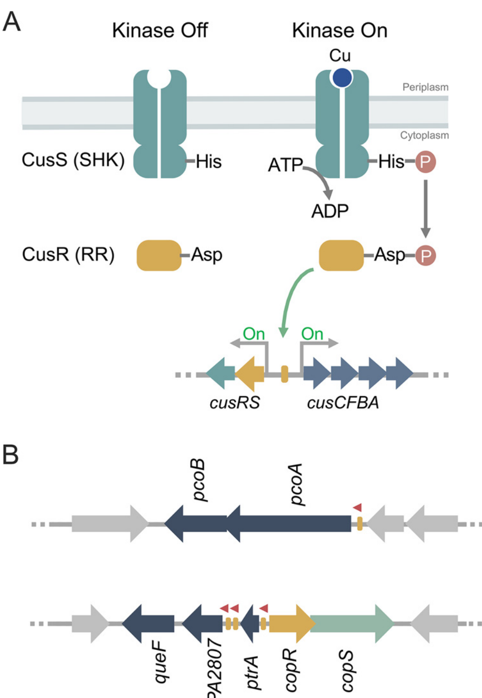

FIG 1 Transcriptional control mediated by TCSs. (A) Activation dynamics of canonical TCSs exemplified with the *E. coli* Cu-sensing CusRS. (B) Scheme of the TCS *P. aeruginosa* CopRS regulon. Promoter regions recognized by CopR (yellow rectangles) and transcription direction (red arrowheads) are shown. Overlapping arrows indicate that the start codon of second gene overlaps the stop codon of first gene in both *pcoAB* and *copRS* operons.

transporter is not part of the CopRS regulon but is rather controlled by the cytoplasmic Cu^{+} sensor CueR (9). Given the distinct architecture of the *P. aeruginosa* CopRS regulon, a distinct sensing/activating mechanism for the control of periplasmic Cu^{+} homeostasis in *Pseudomonas* could be expected.

The structure of the isolated periplasmic domain of *E. coli* CusS shows four Ag^{+} (acting as Cu^{+} analog) binding sites per dimer (47). Two sites are symmetrically located at the dimer interface, and two are situated in outer loops of separated monomers. Reported estimates of metal-sensor affinities are limited and quite dissimilar among the different Cu-sensor histidine kinases. The *E. coli* CusS interacts with Ag^{+} with an affinity in the micromolar range (48), while *Synechocystis* CopS binds Cu^{2+} with high subattomolar affinity (32). Thus, significant aspects of sensor activation such as selectivity (Cu^{+} versus Cu^{2+}) and sensitivity (affinity) are still undefined. These parameters will determine the level of free Cu in the periplasm and provide evidence for the metal redox status.

Here, we report that the transcriptional control of the CopRS regulon in *P. aeruginosa* relies on the Cu-dependent phosphatase activity of CopS, rather than on its kinase activity. Phosphorylation of the RR CopR and the consequent activation of the CopRS regulon appear independent of CopS. However, in the absence of Cu, CopS shuts down the transcriptional response to Cu^{+}, likely dephosphorylating CopR. Then, when the periplasmic Cu^{+} level rises, the phosphatase activity of CopS is blocked, allowing the accumulation of phosphorylated CopR (CopR~P) which promotes the expression of the periplasmic Cu^{+}-homeostasis network. Finally, CopS binds both Cu^{+} and Cu^{2+} with similar high affinities, ensuring the absence of free Cu in the periplasm.

RESULTS

CopRS controls *P. aeruginosa* periplasmic Cu^{+} homeostasis (9). Notably, there are significant differences between the CopRS regulon and those of other characterized

Downloaded from http://msphere.asm.org/ on December 23, 2020 by guest

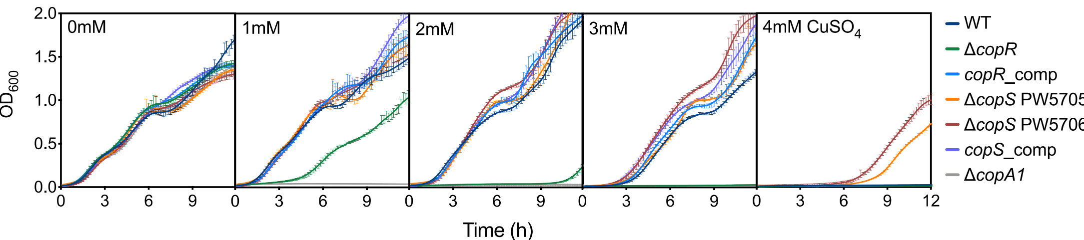

FIG 2 Cu tolerance of Δ*copR* and Δ*copS* mutant strains. Growth rate of WT, Δ*copR*, Δ*copS* (PW5705 and PW5706), Δ*copA1*, and CopR and CopS complemented strains in the absence or the presence of increasing (0 to 4 mM) concentrations of $CuSO_4$. Data are the mean ± SEM from at least three independent experiments.

Cu^{+}-sensing TCSs, e.g., *E. coli* CusRS. The likely presence of additional mechanistic and molecular differences warranted a closer examination of CopRS function.

Deletion of *copS* leads to Cu tolerance. We initiated our studies by looking at the growth rate of Δ*copS* and Δ*copR* mutant strains in the presence of external Cu^{2+}. Based on the mechanism of described Cu^{+}-sensing TCSs (Fig. 1A), it was expected that the lack of either CopS or CopR would lower the cellular tolerance to external Cu^{2+}. As anticipated, the Δ*copR* strain was more susceptible to Cu^{2+} than the wild-type (WT) strain (Fig. 2). In contrast, two independent *copS* transposon mutants, PW5705 and PW5706 (see Fig. S1 in the supplemental material), were surprisingly much more tolerant to external Cu^{2+} than the WT strain. As these phenotypes were reversed by complementation with the corresponding gene, all subsequent experiments were performed with the Δ*copS* PW5706 strain. For comparison, in addition to the WT strain, the well-characterized Cu^{+}-sensitive Δ*copA1* mutant strain was included as a control in this initial phenotypical characterization (8).

Importantly, these growth phenotypes were the consequence of significantly different levels of intracellular Cu^{+} upon exposure to $CuSO_4$ (Fig. 3). Thus, the Δ*copR* mutant strain accumulated more Cu^{+}, while the Δ*copS* cells stored less metal, than the WT strain. Again, alterations in Cu^{+} levels were reversed by gene complementation of the mutant strains. These differences in Cu tolerance and cellular metal levels observed for the Δ*copR* and Δ*copS* mutant strains cannot be explained by the currently accepted model derived from the *E. coli* TCS CusRS (Fig. 1A) and suggest an alternative mechanism for coupling periplasmic Cu^{+} sensing and gene expression in *P. aeruginosa*.

The CopRS regulon is expressed in the Δ*copS* mutant strain independently of the Cu^{+} levels. Toward understanding the increased Cu tolerance and intracellular levels in the Δ*copS* strain, we investigated the transcriptional response to Cu^{2+} exposure of the CopRS regulon in the Δ*copR* and Δ*copS* mutant strains. We have described that CopRS controls the expression of *pcoA*, *pcoB*, *ptrA*, *queF*, and *PA2807* coding for periplasmic and outer membrane proteins (Fig. 1B) (9). As previously observed in the WT strain, genes of the CopRS regulon are induced in response to external Cu^{2+} exposure (Fig. 4). As expected, their Cu-induced expression was abolished in the Δ*copR* mutant. In contrast, the Δ*copS* mutant strain showed a constitutive activation of all the genes of the CopRS regulon, even in the absence of the Cu^{2+} stimulus. In the Δ*copS* background, expression of these genes was maximal and independent of the presence of Cu^{2+} in the culture medium. That similar expression pattern of the CopRS-activated genes in the Δ*copS* strain was attained in the absence of added Cu^{2+} and in the presence of low, nondeleterious Cu^{2+} levels (0.5 mM), intermediate toxic Cu^{2+} levels (2 mM), and lethal Cu^{2+} levels (4 mM) (Fig. S2). This suggests that CopS is not required to activate, i.e., phosphorylate, CopR. The activation of CopR in the Δ*copS* mutant in the absence of supplemented Cu^{2+} points to a mechanism where the phosphatase activity of CopS maintains low levels of CopR~P under noninducing conditions. The Δ*copS* strain failure to maintain the system *off* in the absence of added Cu was reversed in the complemented strain (Fig. 4). The transcriptional analyses also showed that the expression of the *copRS* operon is not autoregulated (Fig. S3). That is, even

Downloaded from http://msphere.asm.org/ on December 23, 2020 by guest

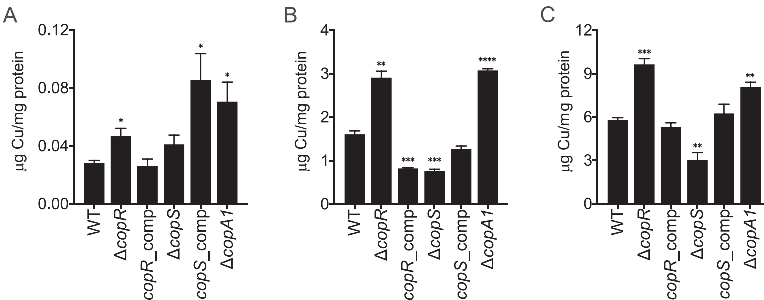

FIG 3 Whole-cell Cu levels in WT, Δ*copR*, Δ*copS*, Δ*copA1*, and CopR and CopS complemented strains under normal growth conditions (i.e., no additional $CuSO_4$ added) (A) and after 10 min exposure to 2 mM $CuSO_4$ (B) or 4 mM $CuSO_4$ (C). Data are the mean ± SEM from three independent experiments. Significant differences from values with the WT strain as determined by unpaired two-tailed Student's *t* test are *, $P < 0.05$; **, $P < 0.01$; ***, $P < 0.001$; ****, $P < 0.0001$.

though *copRS* expression is induced in response to Cu^{+}, it was not affected either in the Δ*copR* or in the Δ*copS* mutant strain. Noticeably, the repressed transcription of *oprC*, coding for the outer membrane Cu importer (9, 49), was further repressed in the Δ*copS* mutant strain, consistent with the Cu^{+}-tolerant phenotype, i.e., less intracellular Cu, exhibited by this strain (Fig. S4A). Conversely, the increased transcription of genes in the CueR regulon (*copA1* and *cusA*) in response to Cu^{+} was not altered either in the Δ*copR* or in the Δ*copS* mutant strain (Fig. S4B). This confirms that the lack of transcriptional control observed in the Δ*copR* and Δ*copS* mutant strains is limited to the genes of the CopRS regulon. Maximal transcription of the CopRS-activated genes in the Δ*copS* strain, even in the absence of external Cu^{2+} stress, requires CopR~P. As mentioned before, RRs can be phosphorylated either by alternative kinases or metabolically, by physiologically relevant small phosphodonors like the acetyl phosphate pool (39–43). This pool, in turn, depends on the activity of two enzymes, the phosphate acetyltransferase Pta and the acetate kinase AckA. Testing the role of acetyl phosphate on

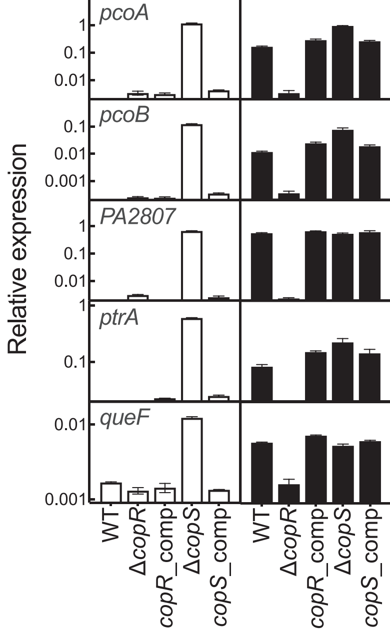

FIG 4 Expression of genes in the CopRS regulon in WT, Δ*copR*, Δ*copS*, and corresponding complemented strains in the absence (white) and the presence (black) of 0.5 mM $CuSO_4$ (5-min treatment). Transcript levels of *pcoA*, *pcoB*, *PA2807*, *ptrA*, and *queF* genes are plotted relative to that of the housekeeping gene *PA4268*. Data are the mean ± SEM from three independent experiments.

Downloaded from http://msphere.asm.org/ on December 23, 2020 by guest

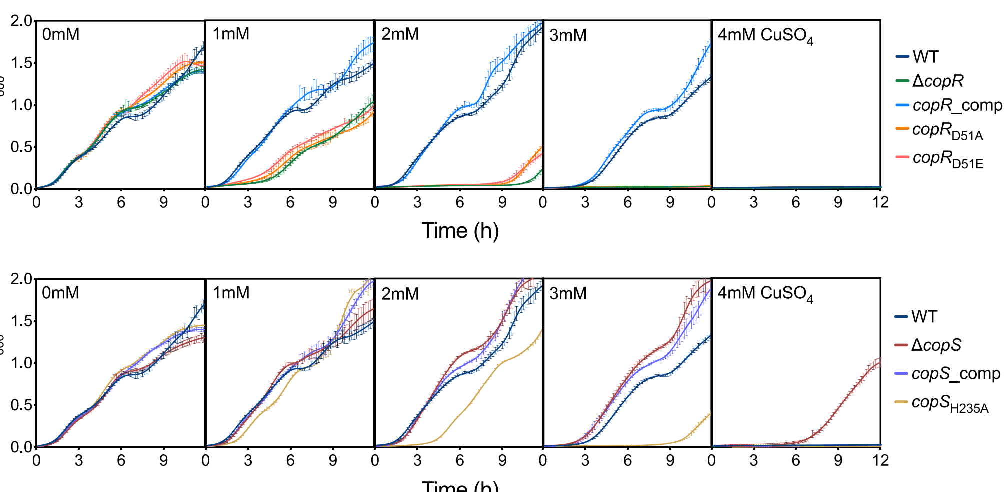

FIG 5 Cu tolerance of Δ*copR* and Δ*copS* mutant strains complemented with CopR and CopS mutant proteins lacking the phosphorylatable residues. (A) Growth rate of the Δ*copR* mutant complemented with $copR_{D51A}$ or $copR_{D51E}$ in the absence or the presence of increasing (0 to 4 mM) concentrations of $CuSO_4$. (B) Growth rate of the Δ*copS* mutant complemented with $copS_{H235A}$ in the presence of 0 to 4 mM $CuSO_4$. Data are the mean ± SEM from three independent experiments.

CopR phosphorylation, the Cu^{2+} resistance of the Δ*pta* and Δ*ackA* strains was evaluated (Fig. S5). Both strains showed a Cu^{2+} sensitivity profile similar to that of the WT strain, suggesting that phosphorylation of CopR does not depend on the acetyl phosphate pool and the involvement of a yet-unidentified SHK.

His_{235} acts as a switch to turn on/off the CopS signaling pathway. The cytoplasmic region of the SHK sensory proteins contains the catalytic domain and the phosphotransfer domain able to switch between kinase and phosphatase activities in a signal-dependent manner (42, 50). In most SHKs, this phosphotransfer domain contains an invariant His residue that autophosphorylates in the first step of the signaling cascade, activating the kinase state of the SHK. Subsequently, the RR protein is phosphorylated in a highly conserved phosphoacceptor Asp, leading to the transcriptional induction of its activated genes (51) (Fig. 1A). In contrast to the kinase state, in the phosphatase state a dephosphorylated SHK removes the phosphate group from the RR (42). The kinase and phosphatase states are mutually exclusive. In some cases, the activation of the kinase state is associated with phosphatase deactivation with the consequent accumulation of phosphorylated RR. The observed phenotypes in Δ*copS* and Δ*copR* strains suggest that in the absence of Cu^{+}, CopS acts as a phosphatase dephosphorylating CopR~P. Then, when CopS senses Cu^{+}, its phosphatase would be inactivated, leading to a rise of CopR~P, triggering the expression of the CopRS regulon. Testing these ideas, the phosphorylatable residues, His_{235} in CopS and Asp_{51} in CopR, were identified by sequence alignment with characterized TCS (Fig. S6). Site-directed mutagenesis was performed to generate Asp_{51}Ala and Asp_{51}Glu replacements in CopR and His_{235}Ala in CopS coding sequences, and the resulting constructs were employed to complement the corresponding Δ*copR* and Δ*copS* mutant strains.

Figure 5A shows that the mutations Asp_{51}Ala and Asp_{51}Glu in CopR lead to growth phenotypes comparable to that of the Δ*copR* strain. This pointed to the requirement of Asp at this position for CopR function and revealed that the Glu residue does not act as a phosphomimetic residue. In agreement, Fig. 6 shows that neither $CopR_{D51A}$ nor $CopR_{D51E}$ was able to activate *pcoB* expression in the presence of external Cu^{2+}, a lack of function associated with the absence of the Asp_{51} phosphorylation. Conversely, the His_{235}Ala CopS mutant behaved differently from both the WT and the Δ*copS* strain. In contrast to the Cu^{2+} tolerance phenotype observed for the Δ*copS* mutant, the His_{235}Ala CopS mutant had an increased sensitivity to Cu^{2+} (Fig. 5B), suggesting that the phosphatase activity of CopS remains functional in the absence of His_{235}. Analysis

Downloaded from http://msphere.asm.org/ on December 23, 2020 by guest

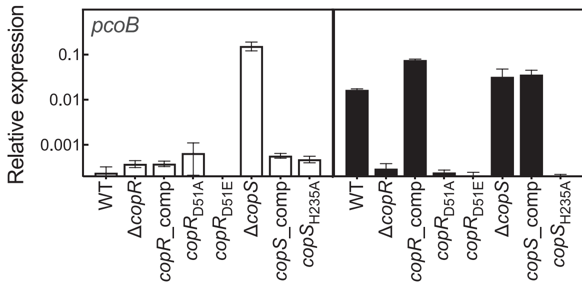

FIG 6 Expression of *pcoB* in Δ*copR* and Δ*copS* mutant strains complemented with CopR and CopS lacking the phosphorylatable residues. *pcoB* expression was determined in the absence (white) and the presence (black) of 2 mM $CuSO_4$ (5-min treatment) in the indicated strains. The Δ*copR* mutant was complemented with *copR* coding for substitutions Asp_{51}Ala and Asp_{51}Glu. The Δ*copS* mutant was complemented with the *copS* gene coding for substitution His_{235}Ala. Transcript levels of *pcoB* are plotted relative to the housekeeping gene *PA4268*. Data are the mean ± SEM from three independent experiments.

of the transcriptional activation of genes in the CopRS regulon further supports this idea. In the absence of supplemented Cu^{2+}, *pcoB* transcription remained low in the His_{235}Ala CopS mutant, similar to the level observed in the WT strain and in contrast to the increased expression in the Δ*copS* mutant strain. In fact, addition of external Cu^{2+} did not promote the transcription of *pcoB* in the His_{235}Ala mutant, similar to the *pcoB* expression pattern in the Δ*copR* strain and clearly different from the induction observed in the WT and the maximal expression attained in the Δ*copS* mutant. The more marked *pcoB* expression defect under Cu stress of the *copS*$_{H235A}$ strain compared to the Δ*copR* strain is likely associated with experimental conditions. Importantly, the lack of transcriptional activation of *pcoB* suggests that the His_{235}Ala CopS mutant was not able to respond to changes in periplasmic Cu^+ levels, explaining the Cu^{2+}-sensitive phenotype observed for this strain (Fig. 5B) and suggesting that the His_{235}Ala mutation locked CopS in a phosphatase-ON state irresponsive to the presence of Cu.

CopS periplasmic sensor domain binds two Cu^+ ions per functional unit. Most TCS sensors are homodimeric membrane proteins. The periplasmic sensor domain of CopS, flanked by two transmembrane segments (Fig. S1), extends between residues 34 and 151 [$CopS_{(34–151)}$]. The function of the system relies on its ability to bind cognate metal ions. To explore CopS metal binding properties, the *P. aeruginosa* $CopS_{(34–151)}$ sensor domain carrying alternative His or Strep tags was heterologously expressed and purified to homogeneity (Fig. S7). His-tagged proteins were used in Cu^+ binding, while the Strep-tagged fragments were used in Cu^{2+} binding experiments.

The Cu^+ binding stoichiometry of the isolated domain was first measured at a saturating metal concentration (five times molar excess) in the presence of dithiothreitol (DTT) as reducing agent. The $CopS_{(34–151)}$ dimer was able to bind 2.3 ± 0.5 Cu^+. This differs from the stoichiometry of four Ag^+ (used as Cu^+ analog) per dimer observed in *E. coli* CusS (47). However, the periplasmic sensor domain of CopS homolog proteins is considerably shorter than the CusS domain, lacking a loop containing residues (Ser_{84}, Met_{133}, Met_{135}, and His_{145}) involved in metal binding in CusS (Fig. S6B). In effect, a phylogenetic tree built with sequences homologous to CopS and CusS (>45% identity) shows a clear evolution of two distinct subgroups of CusS homologs in *Enterobacterales* and in *Burkholderiales* and a separate group of CopS homologs in *Pseudomonadales* (Fig. S8). This structural difference leading to the alternative stoichiometry can be more easily observed when the homology modeling of *P. aeruginosa* CopS is overlapped with the crystal structure of the Ag^+-bound periplasmic sensor domain of *E. coli* CusS (47) (Fig. 7). The two symmetric metal binding sites fully conserved in both CopS and CusS are located at the dimeric interface. Each site is formed by two invariant His residues (His_{41} and His_{140} in CopS), one from each dimer subunit. A Phe residue likely interacting with the metal in CusS is also conserved in CopS (Phe_{42}). These are probably the Cu^+-sensing

Downloaded from http://msphere.asm.org/ on December 23, 2020 by guest

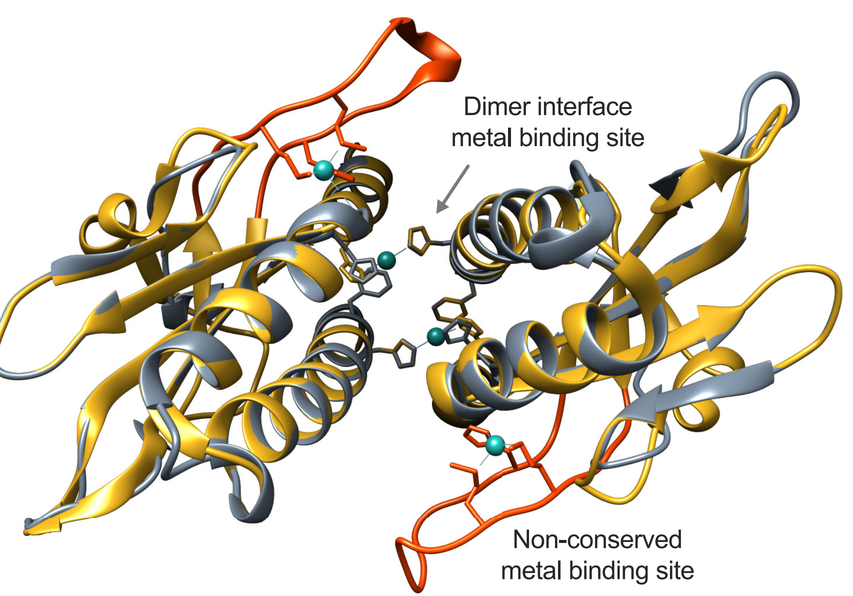

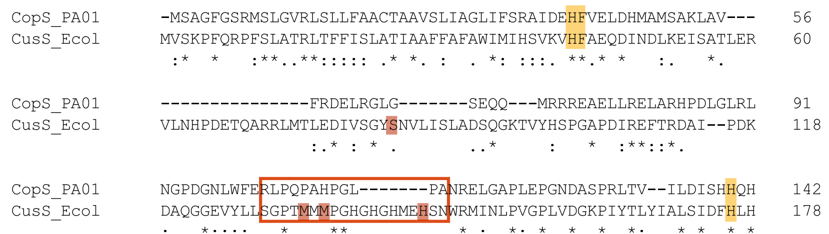

FIG 7 Structural superposition of the periplasmic Cu^+ binding loop of *P. aeruginosa* CopS (gray) and *E. coli* CusS (yellow). The structure of CopS was modeled using the CusS structure as the template (PDB ID: 5KU5 [43]). An overall root mean square deviation of 0.791 Å (Cα atoms) was calculated for the superposition of CopS and CusS structures. Conserved Cu binding sites at the dimeric interface (His_{41}, Phe_{42}, and His_{140}) are shown as sticks in the structural model and highlighted in yellow in the sequence alignment. The Cu^+ binding sites within the CusS orange loops (framed in rectangle in the alignment) are not conserved in CopS.

sites involved in signal transduction. On the other hand, the structural comparison clearly shows that the loop containing the additional metal binding sites of CusS is missing in CopS (orange loops, Fig. 7).

The CopS periplasmic sensor binds Cu ions with femtomolar affinities. By analogy with how cytoplasmic sensor metal affinities are tuned to maintain free metal levels (52, 53), the affinity of CopS for Cu^+ ions will certainly have determinant effects on free (hydrated) Cu^+ ion levels in the periplasm. Exploring the binding of Cu^+ to CopS, we measured the sensor metal binding affinity using competing ligands. The ligands were present in excess to ensure effective competition. In all cases, the determinations were performed assuming that both Cu sites at the CopS dimer interface were functionally independent and thermodynamically indistinguishable. Initial determinations of $CopS_{(34–151)}$ affinity for Cu^+ using bathocuproine disulfonate (BCS) as a competitor showed a limited but measurable decrease in the absorbance of the $[Cu^I(BCS)_2{}^{3-}]$ complex, corresponding to a K_D (dissociation constant) value of $CopS_{(34–151)}$ for Cu^+ of 2.2×10^{-14} M (data not shown). However, it was apparent that CopS was not an effective competitor with BCS for the metal. Instead, 2,2′-bicinchoninic acid (BCA), with a lower affinity for copper than that of BCS, appeared more appropriate to measure affinities in the femtomolar range (54). Using BCA as the competing ligand and fitting titration curves to equation 2, a $CopS_{(34–151)}$-Cu^+ K_D of $(2.77 \pm 0.07) \times 10^{-14}$ M

Downloaded from http://msphere.asm.org/ on December 23, 2020 by guest

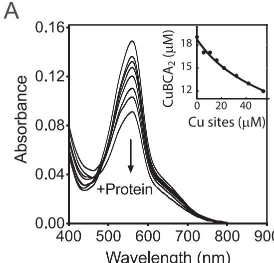

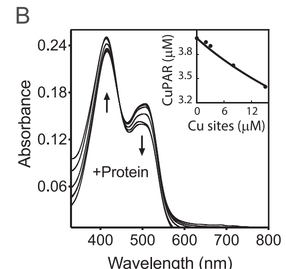

FIG 8 Determination of the dissociation constants K_D of the periplasmic Cu binding loop of $CopS_{(34–151)}$. (A) Spectrophotometric titration of 100 μM BCA and 18.7 μM Cu^+ with 10 to 50 μM His-tagged $CopS_{(34–151)}$. The arrow indicates the decrease in absorbance at 562 nm upon protein addition. The inset shows the fitting of the data set to equation 2 with a K_D of $(2.77 \pm 0.07) \times 10^{-14}$ M (R^2 0.992). Two Cu sites per CopS dimer are assumed. (B) Spectrophotometric titration of 10 μM PAR and 4 μM Cu^{2+} with 2 to 20 μM Strep-tagged $CopS_{(34–151)}$. The arrows indicate the increase in absorbance at 415 nm and the decrease at 562 nm upon protein addition. The inset shows the fitting of the data set to equation 4 with a K_D of $(3.3 \pm 0.1) \times 10^{-14}$ M (R^2 0.984).

was obtained (Fig. 8A). This appears within the range of affinities observed for many other Cu^+ binding molecules (11, 54, 55).

Synechocystis CopS binds Cu^{2+} with high subattomolar affinity (Cu^+ binding stoichiometry was not reported) (32). Exploring the possibility of high-affinity Cu^{2+} binding to *P. aeruginosa* CopS, the chromogenic ligand 4-(2-pyridylazo)resorcinol (PAR) was used as a competitive ligand for Cu^{2+} with purified Strep-tagged $CopS_{(34–151)}$ (Fig. S7), in the absence of reducing agents. A $CopS_{(34–151)}$-Cu^{2+} K_D of $(3.3 \pm 0.1) \times 10^{-14}$ M was observed (Fig. 8B). Consequently, it is apparent that $CopS_{(34–151)}$ binds both Cu^+ and Cu^{2+} with quite similar affinities in the femtomolar range. These high affinities provide insights into the *in vivo* metal dynamics and virtual absence of free Cu ions in the bacterial periplasm.

DISCUSSION

The relevance of the periplasmic Cu pool in the *P. aeruginosa* response to Cu^{2+} stress is well established (10, 56). Results presented here show novel important characteristics of the *P. aeruginosa* TCS CopRS. The sensor has a negative-control mechanism based on its phosphatase rather than on its kinase activity. At the dimer interface, it binds two $Cu^{+/2+}$ ions with femtomolar affinities, likely resulting in the absence of periplasmic free Cu. This CopRS distinct Cu^+ signaling mechanism is in line with the other unique features of the *P. aeruginosa* Cu homeostasis network, namely, cytoplasmic and periplasmic sensors with singular regulons, an RND-transporter regulated by the cytoplasmic sensor, and multiple cytoplasmic Cu^+ chaperones and efflux P_{1B}-ATPases (8–11, 57). The emerging model challenges a number of ideas associated with early studies of the *E. coli* CusRS TCS. Along with *Salmonella*, which has distinct Cu^+ balance mechanisms (6), *P. aeruginosa* provides a clear example of alternative approaches used by bacteria to achieve Cu homeostasis.

CopS Cu-dependent phosphatase activity mediates signal transduction. Characterization of CopRS was initiated by analyzing the tolerance of Δ*copS* and Δ*copR* strains to external Cu^{2+}. While an increased sensitivity was expected based on the reported phenotypes of *E. coli* Δ*cusS* and Δ*cusR* strains, the Δ*copS* strain showed higher tolerance to external Cu^{2+}. Although unexpected, this phenomenon has been previously observed, albeit unnoticed. It was reported that deletion of the *P. aeruginosa* CopS did not compromise the ability of the bacteria to grow in the presence of Cu^{2+} (58). Furthermore, there was no evident Cu-induced expression of a *lacZ* transcriptional fusion to a *Pseudomonas putida* CinRS (a CopRS ortholog)-dependent promoter in a *P. aeruginosa* Δ*copR* background. However, Cu-independent expression of the same reporter was attained in the *P. aeruginosa* Δ*copS* background (59). Also similar to the *P.*

Downloaded from http://msphere.asm.org/ on December 23, 2020 by guest

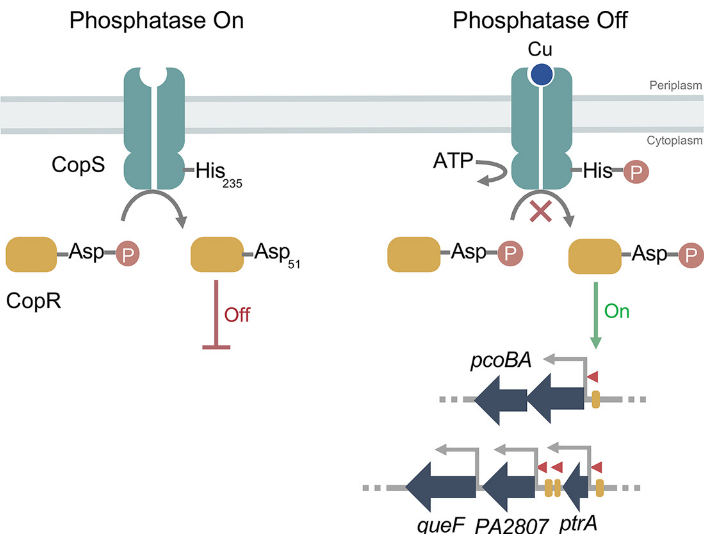

FIG 9 Model of the phosphatase-based mechanism of the *P. aeruginosa* CopRS. Phosphatase On: when periplasmic free Cu remains under the subfemtomolar level, the CopS phosphatase activity maintains low levels of phosphorylated CopR, shutting *off* the transcriptional response to high periplasmic Cu. Phosphatase Off: upon Cu binding, CopS autophosphorylates at His_{235}. This turns *off* the CopS phosphatase activity, allowing the accumulation of phosphorylated CopR and triggering the expression of the CopRS regulon (i.e., *pcoA*, *pcoB*, *queF*, *PA2807*, and *ptrA*).

aeruginosa Δ*copS* strain, a *P. fluorescens* Δ*copS* strain was more tolerant to external Cu^{2+} (36).

The Cu^{2+} resistance phenotype of the *P. aeruginosa* Δ*copS* strain is supported by the maximal expression of the CopRS regulon and the consequent reduced whole-cell Cu^{+} content. The simplest explanation for these observations is a mechanism where, in the absence of Cu, the CopS phosphatase activity abrogates the induction of the CopRS regulon by maintaining low levels of CopR~P (Fig. 9). When CopS detects periplasmic Cu overload, its phosphatase activity is blocked allowing the accumulation of CopR~P, which promotes the expression of the periplasmic Cu homeostasis network.

Signal transduction by archetypical TCSs relies on bifunctional kinase/phosphatase SHKs (60). A positive action results from sensor autokinase activity and phosphotransfer to the RR while negative regulation involves the sensor phosphatase activity (50). The ultimate determining factor of the cascade activation is the phosphorylation status of the RR. Accumulation of RR~P is the consequence of a signal-dependent stimulation of the sensor-kinase activity or a signal-dependent blockage of the sensor-phosphatase activity. While we cannot rule out the absence of autokinase activity, or sensor phosphorylation by an alternative kinase, the most parsimonious model to explain our data is that CopS, under our experimental conditions, harbors autokinase and phosphatase activities. The signal-independent activation of the CopRS regulon in the Δ*copS* background evidences the requirement of the CopS phosphatase activity to maintain low levels of CopR~P in the absence of Cu. It is also apparent that CopS is not required for the phosphorylation of CopR, implying that an alternative mechanism for the phosphorylation of CopR should exist. There is extensive evidence that RRs can be phosphorylated (cross-phosphorylated) by endogenous phosphodonors (39, 41–43). In the case of CopR, acetyl phosphate does not seem to be the donor. Alternative mechanisms for RR phosphorylation known as many-to-one or one-to-many, where many SHKs phosphorylate a given RR or a single SHK phosphorylates multiple RRs, have been proposed (38, 60). It could then be argued that CopR phosphorylation might be the consequence of an unspecific cross talk with a noncognate SHK that occurs only in the absence of CopS. However, such cross talk has been observed only when both the

Downloaded from http://msphere.asm.org/ on December 23, 2020 by guest

reciprocal RR and the cognate SHK were absent (41). These conditions are distinct from those in our experiments.

The evidence indicates that Cu-dependent CopS autokinase activity, or at least the integrity of His_{235}, is required for the inhibition of the CopS-phosphatase activity. His_{235}Ala replacement leads to a Cu^{+}-independent inactivation of the regulon, suggesting a constitutively active phosphatase activity. While this points out that His_{235} is not required for the CopS phosphatase activity, it implies that Cu-dependent CopS autophosphorylation turns *off* the CopS phosphatase activity, leading to accumulation of CopR~P. That is, as described previously, the dephosphorylated SHKs have phosphatase activity (42, 50).

CopS binds two Cu ions with femtomolar affinities. Its Cu binding characteristics are what defines the function of CopS. We determined that *P. aeruginosa* CopS binds two metal ions with an affinity in the 3×10^{-14} M range. Little information is available regarding the binding stoichiometry and affinities of other Cu-sensing TCS sensors. The structure of *E. coli* CusS clearly supports a stoichiometry of four metal atoms per CusS-sensing dimer (47). Two of these ions bind at the dimer interface, while the other two attach to external loops, one in each subunit. Structural comparison of *P. aeruginosa* CopS and *E. coli* CusS shows that both types of sensors would bind and sense the metal with conserved His residues at the dimer interface. However, the CusS extra sites are not conserved in CopS or in its homologs. Regarding binding affinities, *E. coli* CusS binds Ag^{+} with a reported 8 μM affinity, measured in equilibrium dialysis experiments (48); in contrast, *Synechocystis* CopS binds Cu^{2+} with subattomolar affinity (32). It would be quite speculative to compare such dissimilar determinations. However, it might be instructive to consider the observed 10^{-19} to 10^{-21} M affinities of cytoplasmic copper sensors in general (55, 61) and those determined for the cytoplasmic triad CopZ2/CueR/CopZ1 of *P. aeruginosa*, with relative affinities for Cu^{+} ranging between 10^{-15} and 10^{-17} M (9, 11). The weaker affinity of CopS than of the cytoplasmic regulators and chaperones is likely the consequence of a metal binding site formed by His rather than Cys residues. This is a logical arrangement, given the possible oxidation of proximal Cys under periplasmic redox stress. Importantly, a femtomolar affinity still supports the idea that there would not be free $Cu^{+/2+}$ in the cell periplasm, as shown for the cytoplasm (55, 62). However, the relative binding strength of CopS is likely to be linked to those of periplasmic Cu^{+} chaperones that exchange metal with the sensor. That is, the proteins should be able to exchange the metal. However, as shown with cytoplasmic chaperone/sensor partners, the protein-protein binding affinity will have a significant effect in the final exchange constant (11).

CopS binds both Cu^{+} and Cu^{2+} with similar high affinities. It is accepted that cytoplasmic transporters and chaperones bind and distribute cuprous ions. However, the periplasm is a more oxidizing compartment (63, 64), containing enzymes such as the multicopper oxidase PcoA present in the periplasm of *P. aeruginosa* (65). It has been proposed that periplasmic enzymes might catalyze Cu^{+} oxidation to the assumed less toxic Cu^{2+} (66). However, free (hydrated) Cu^{+} would be spontaneously oxidized by O_2 in an aerobic environment. Then, the redox status of periplasmic Cu is unclear and beyond the goals of this report. We presume that Cu oxidation state will depend on the molecule interacting with and delivering Cu to CopS. In any case, the capability to bind both Cu^{+} and Cu^{2+} might help CopS to sense the metal under redox stress.

The distinct CopRS mechanism is in line with the singular architecture of the *P. aeruginosa* Cu homeostasis system. *E. coli* and *Salmonella* are the frequent models to explore transition metal homeostasis in Gram-negative bacteria. However, recent studies of *P. aeruginosa* have begun to show different novel molecular strategies to sense, buffer, and distribute Cu^{+} (8–10, 67). For instance, consider how the regulons of both compartmental sensors, CopRS and CueR, differ among these three organisms (6, 9, 24, 68, 69). Also, analyze the multiple functionally distinct homologous Cu^{+} ATPases present in *Salmonella* and *Pseudomonas* and how these three Gram-negative bacteria have solved cytoplasmic Cu^{+}-chaperoning using alternative strategies (6, 11, 70). Along with these observations, the relevance of periplasmic Cu^{+} sensing, storage, and transport

Downloaded from http://msphere.asm.org/ on December 23, 2020 by guest

has become more apparent. Then, it is not surprising that these model systems solve periplasmic Cu^{+} sensing either via a kinase sensor (CusRS, *E. coli*), an integration of a cytoplasmic Cu sensor with a general envelope stress response TCS (CueR-CpxRS, *Salmonella* [71]) or a phosphatase sensor (CopRS, *P. aeruginosa*). The evolutive and ecological advantages of these systems are still to be discovered and will be the subject of future enquiries in the field.

MATERIALS AND METHODS

Bacterial strains, plasmids, and growth conditions. Bacterial strains, plasmids, and primers used in this study are listed in Table S1 in the supplemental material. *P. aeruginosa* PAO1 served as WT strain. Mutant strains PW5704 (Δ*copR*), PW5705 (Δ*copS*), PW5706 (Δ*copS*), PW2519 (Δ*pta*), and PW2520 (Δ*ackA*) were obtained from the *P. aeruginosa* PAO1 transposon mutant library (University of Washington, Seattle, WA) (72, 73). *P. aeruginosa* strains were grown at 37°C in Luria-Bertani (LB) medium supplemented with 25 μg/ml Irgasan, 30 μg/ml tetracycline (mutant strains), or 30 μg/ml gentamicin (complemented strains). *E. coli* strains were grown at 37°C in LB medium supplemented with 100 μg/ml ampicillin, 30 μg/ml kanamycin, or 10 μg/ml gentamicin, depending on the plasmid selection.

Construction of *P. aeruginosa* complemented strains. Mutant strains were complemented with the corresponding gene under the control of the native promoter using the mini-Tn7T insertion system (74). Briefly, the genes and their 500-bp upstream promoter regions were amplified by PCR. The 3′ primer included a His_6 tag coding sequence. Amplicons were cloned into the pUC18-mini-Tn7T-Gm suicide delivery vector. These plasmids were used as the template to introduce mutations coding for single substitutions $copR_{D51A}$, $copR_{D51E}$, and $copS_{H235A}$ using Gibson assembly (75). The resulting plasmids were then introduced into recipient strains by conjugation, using the helper strains SM10(λpir)/pTNS2 and HB101/pRK2013. Conjugants were selected on 30 μg/ml gentamicin-25-μg/ml Irgasan-LB plates. Complemented strains were verified by PCR.

Cu^{2+} sensitivity assay. Overnight cultures were diluted in 25 μg/ml Irgasan-LB medium, adjusted to an optical density at 600 nm (OD_{600}) of 0.05, and supplemented with the indicated $CuSO_4$ concentration. Cell growth in 0.2 ml liquid medium was monitored for 24 h (OD_{600}) at 37°C with continuous shaking using an Epoch 2 microplate spectrophotometer (BioTek).

Whole-cell Cu content. Cells (mid-log phase) were incubated in LB medium supplemented with 0.5, 2, or 4 mM $CuSO_4$. Aliquots were taken after 10 min, treated with two times molar excesses of DTT and BCS, and harvested by centrifugation at 17,000 × *g*, 1 min. Pellets were washed twice with 150 mM NaCl and mineralized with fuming HNO_3 (trace metal grade) for 60 min at 80°C and 2 M H_2O_2 for 60 min at room temperature. Cu levels were measured using atomic absorption spectroscopy (AAS) as described previously (9).

Gene expression analysis. Cells (mid-log phase) were incubated in antibiotic-free LB medium supplemented with 0.5, 2, or 4 mM $CuSO_4$. In all cases, 0.5-ml aliquots were taken at 5 min and stabilized with RNAprotect bacterial reagent (Qiagen), and RNA was isolated with the RNeasy minikit (Qiagen). RNA was treated with DNase I, purified by phenol-chloroform extraction, and ethanol precipitated. One microgram of RNA was used for cDNA synthesis using the ProtoScript II kit (New England BioLabs). qPCRs were carried out with FastStart Essential DNA Green Master (Roche) in a 10-μl final volume, using 0.25 μM (each) primer (Table S1). The efficiency of primer sets was evaluated by qPCR in serial dilutions of WT cDNA. Results were normalized to 30S ribosomal protein S12 (*PA4268*) (8).

Protein expression and purification. The DNA fragment encoding the periplasmic copper binding loop of $CopS_{(34–151)}$ was amplified from genomic DNA using 3′-end primers that introduced sequences encoding either a Strep tag or a His_6 tag joined by a tobacco etch virus (TEV) cleavage site (Table S1). The His-tagged protein had a higher expression yield and was used in Cu^{+} binding experiments since this tag does not bind monovalent Cu^{+}. However, the His tag binds Cu^{2+}. Cleavage of the His tag was not pursued because the CopS (dimer) and the TEV have exactly the same molecular weight and it is not possible to ensure full cleavage. In consequence, a Strep-tagged protein was used in Cu^{2+} binding experiments. Resulting amplicons were cloned in the pBAD-topo vector (Invitrogen) and expressed in *E. coli* LMG194 cells. His-tagged $CopS_{(34–151)}$ was purified using Ni-NTA columns (Roche) (11). Strep-tagged $CopS_{(34–151)}$ was affinity purified using Strep-Tactin XT Superflow columns (IBA) (11). Purified proteins were stored in 20% glycerol, 25 mM Tris (pH 8), 100 mM sucrose, 150 mM NaCl at −80°C. Protein concentrations were determined in accordance with work of Bradford (76), and purity was estimated by SDS-PAGE followed by Coomassie brilliant blue staining (Fig. S7). Proteins were purified as ≥90% *apo* forms as confirmed by AAS.

Copper binding determinations. $CopS_{(34–151)}$-Cu^{+} binding stoichiometry was determined by incubating $CopS_{(34–151)}$ His-tagged protein with five times molar excess of $CuSO_4$ in 25 mM HEPES, pH 8, 150 mM NaCl, 0.5 mM DTT for 10 min at room temperature with gentle agitation. DTT was included to reduce Cu^{2+} to Cu^{+} and prevent protein precipitation that occurs upon addition of excess Cu^{+} using ascorbate. This is a common observation when purified proteins are exposed to Cu and is usually solved, as in this case, by replacing the reducing agent. Unbound Cu^{+} was removed by passage through a Sephadex G-10 column (GE Healthcare) followed by two washing steps using a 3-kDa Centricon. The amount of Cu^{+} bound to protein was determined by AAS.

$CopS_{(34–151)}$-Cu^{+} dissociation constants (K_D) were determined by competition assays with the chromogenic ligands BCS {$[Cu^{I}(BCS)_2]^{3-}$ β_2' formation constant $10^{20.8}$ M^{-2}, $\varepsilon_{483\ nm}$ 13,000 M^{-1} cm^{-1}} and BCA {$[Cu^{I}(BCA)_2]^{3-}$ β_2' formation constant $10^{17.7}$ M^{-2}, $\varepsilon_{562\ nm}$ 7,900 M^{-1} cm^{-1} [77]}. Cu^{+} solutions were

Downloaded from http://msphere.asm.org/ on December 23, 2020 by guest

generated from $CuSO_4$ in the presence of large excess ascorbate and NaCl, which stabilizes Cu^+ as $[Cu^{I}Cl_n]^{(17-n)-}$ (78). Briefly, for BCS competitions, 10 μM Cu^+, 25 μM BCS in buffer 25 mM HEPES, pH 8, 150 mM NaCl, 10 mM ascorbic acid were titrated with 10 to 50 μM His-tagged $CopS_{(34-151)}$ and incubated for 5 min at room temperature, and the 300- to 800-nm absorption spectra were recorded. The same protocol was used for BCA competitions using 18.7 μM Cu^+, 100 μM BCA, and 5 to 50 μM protein instead. $CopS_{(34-151)}$-Cu^+ K_Ds were calculated by curve-fitting of the experimental data to the equilibrium in equations 1 and 2 (54).

$$MP + 2L' \leftrightharpoons ML_2 + P \tag{1}$$

$$K_D\beta_2' = \frac{([P]_{\text{total}}/[MP]) - 1}{\{([L]_{\text{total}}/[ML_2]) - 2\}^2 [ML_2]} \tag{2}$$

$CopS_{(34-151)}$-Cu^{2+} K_Ds were determined using the indicator PAR as competitor ($[Cu^{II}(PAR)]$ conditional K_A' formation constant for Cu^{2+} at pH 7.4 of $10^{14.6}$ M^{-1}, isosbestic point $A_{445\ nm}$, $\varepsilon_{505\ nm}$ 41,500 M^{-1} cm^{-1} [79]). Four micromolar Cu^+, 10 μM PAR in buffer 20 mM HEPES, pH 7.4, 150 mM NaCl were titrated with 2 to 20 μM Strep-tagged $CopS_{(34-151)}$ and incubated at room temperature to equilibrate until no further spectral changes were observed (60 min), and the 300- to 800-nm absorption spectra were recorded. The K_D value was obtained from a curve-fitting of a series of experimental data to equations 3 and 4. Reported errors are asymptotic standard errors provided by the fitting software (Kaleidagraph; Synergy).

$$MP + L' \leftrightharpoons ML + P \tag{3}$$

$$K_D K_A' = \frac{([P]_{\text{total}}/[MP]) - 1}{([L]_{\text{total}}/[ML]) - 1} \tag{4}$$

Bioinformatic approaches. In general, protein sequences were retrieved from UniProt (80) and aligned using Clustal Omega (81). To build the phylogenetic trees, the full-length protein sequences of *E. coli* CusS and *P. aeruginosa* CopS sequences were independently used as query to search for homologs in the UniProtKB database using the UniProt/BLAST tool. Sequences more than 45% identical over their entire lengths were retrieved and aligned. Phylogenetic trees were calculated with the Jalview software (82), using the distance matrix BLOSUM62 and the Average Distance (unweighted pair group method using average linkages [UPGMA]) algorithm.

The structure of the soluble periplasmic copper binding loop of $CopS_{(34-151)}$ was modeled using the online server SWISS-MODEL (83) and the structure of the *E. coli* CusS soluble periplasmic domain (PDB ID: 5KU5) (47) as the template. Conserved metal binding residues of CopS were identified by superimposing its structure with 5KU5 using UCSF Chimera (84).

SUPPLEMENTAL MATERIAL

Supplemental material is available online only.

FIG S1, PDF file, 0.2 MB.
FIG S2, PDF file, 0.04 MB.
FIG S3, PDF file, 0.03 MB.
FIG S4, PDF file, 0.04 MB.
FIG S5, PDF file, 0.1 MB.
FIG S6, PDF file, 0.1 MB.
FIG S7, PDF file, 1.1 MB.
FIG S8, PDF file, 0.1 MB.
TABLE S1, PDF file, 0.1 MB.

ACKNOWLEDGMENTS

This work was supported by grant R01GM114949 from the National Institutes of Health to J.M.A. F.C.S. is a career investigator of CONICET and the Rosario National University Research Council.

Author contributions: L.N.-A. and C.X. performed research; L.N.-A., F.C.S., and J.M.A. designed research, analyzed data, and wrote the paper.

We declare no competing interest.

REFERENCES

1. Argüello JM, Raimunda D, Padilla-Benavides T. 2013. Mechanisms of copper homeostasis in bacteria. Front Cell Infect Microbiol 3:73. https://doi.org/10.3389/fcimb.2013.00073.
2. Fraústo da Silva JJR, Williams RJP. 2001. The biological chemistry of the elements: the inorganic chemistry of life, 2nd ed. Oxford University Press, Oxford, United Kingdom.

Downloaded from http://msphere.asm.org/ on December 23, 2020 by guest

3. Macomber L, Imlay JA. 2009. The iron-sulfur clusters of dehydratases are primary intracellular targets of copper toxicity. Proc Natl Acad Sci U S A 106:8344–8349. https://doi.org/10.1073/pnas.0812808106.
4. Dupont CL, Grass G, Rensing C. 2011. Copper toxicity and the origin of bacterial resistance-new insights and applications. Metallomics 3:1109–1118. https://doi.org/10.1039/c1mt00107h.
5. Osman D, Cavet JS. 2008. Copper homeostasis in bacteria. Adv Appl Microbiol 65:217–247. https://doi.org/10.1016/S0065-2164(08)00608-4.
6. Pontel LB, Soncini FC. 2009. Alternative periplasmic copper-resistance mechanisms in Gram negative bacteria. Mol Microbiol 73:212–225. https://doi.org/10.1111/j.1365-2958.2009.06763.x.
7. Espariz M, Checa SK, Audero ME, Pontel LB, Soncini FC. 2007. Dissecting the *Salmonella* response to copper. Microbiology (Reading) 153:2989–2997. https://doi.org/10.1099/mic.0.2007/006536-0.
8. González-Guerrero M, Raimunda D, Cheng X, Argüello JM. 2010. Distinct functional roles of homologous Cu^+ efflux ATPases in *Pseudomonas aeruginosa*. Mol Microbiol 78:1246–1258. https://doi.org/10.1111/j.1365-2958.2010.07402.x.
9. Quintana J, Novoa-Aponte L, Argüello JM. 2017. Copper homeostasis networks in the bacterium *Pseudomonas aeruginosa*. J Biol Chem 292:15691–15704. https://doi.org/10.1074/jbc.M117.804492.
10. Parmar JH, Quintana J, Ramírez D, Laubenbacher R, Argüello JM, Mendes P. 2018. An important role for periplasmic storage in *Pseudomonas aeruginosa* copper homeostasis revealed by a combined experimental and computational modeling study. Mol Microbiol 110:357–369. https://doi.org/10.1111/mmi.14086.
11. Novoa-Aponte L, Ramírez D, Argüello JM. 2019. The interplay of the metallosensor CueR with two distinct CopZ chaperones defines copper homeostasis in *Pseudomonas aeruginosa*. J Biol Chem 294:4934–4945. https://doi.org/10.1074/jbc.RA118.006316.
12. Lohmeyer E, Schroder S, Pawlik G, Trasnea PI, Peters A, Daldal F, Koch HG. 2012. The ScoI homologue SenC is a copper binding protein that interacts directly with the *cbb(3)*-type cytochrome oxidase in *Rhodobacter capsulatus*. Biochim Biophys Acta 1817:2005–2015. https://doi.org/10.1016/j.bbabio.2012.06.621.
13. Ekici S, Turkarslan S, Pawlik G, Dancis A, Baliga NS, Koch HG, Daldal F. 2014. Intracytoplasmic copper homeostasis controls cytochrome c oxidase production. mBio 5:e01055-13. https://doi.org/10.1128/mBio.01055-13.
14. Trasnea PI, Andrei A, Marckmann D, Utz M, Khalfaoui-Hassani B, Selamoglu N, Daldal F, Koch HG. 2018. A copper relay system involving two periplasmic chaperones drives cbb3-type cytochrome c oxidase biogenesis in *Rhodobacter capsulatus*. ACS Chem Biol 13:1388–1397. https://doi.org/10.1021/acschembio.8b00293.
15. Pontel LB, Scampoli NL, Porwollik S, Checa SK, McClelland M, Soncini FC. 2014. Identification of a *Salmonella* ancillary copper detoxification mechanism by a comparative analysis of the genome-wide transcriptional response to copper and zinc excess. Microbiology (Reading) 160:1659–1669. https://doi.org/10.1099/mic.0.080473-0.
16. Argüello JM, Padilla-Benavides T, Collins JM. 2013. Transport mechanism and cellular functions of bacterial Cu^+-ATPases, p 155–162. *In* Culotta V, Scott JA (ed), Metals in cells. Encyclopedia of inorganic and bioinorganic chemistry. Wiley & Sons, Ltd, Chichester, United Kingdom.
17. Stewart LJ, Thaqi D, Kobe B, McEwan AG, Waldron KJ, Djoko KY. 2019. Handling of nutrient copper in the bacterial envelope. Metallomics 11:50–63. https://doi.org/10.1039/c8mt00218e.
18. Neyrolles O, Wolschendorf F, Mitra A, Niederweis M. 2015. Mycobacteria, metals, and the macrophage. Immunol Rev 264:249–263. https://doi.org/10.1111/imr.12265.
19. Solioz M. 2018. Copper and bacteria: evolution, homeostasis and toxicity, p 49–80. Springer International Publishing, Cham, Switzerland.
20. Ladomersky E, Petris MJ. 2015. Copper tolerance and virulence in bacteria. Metallomics 7:957–964. https://doi.org/10.1039/c4mt00327f.
21. Hernández-Montes G, Argüello JM, Valderrama B. 2012. Evolution and diversity of periplasmic proteins involved in copper homeostasis in gamma proteobacteria. BMC Microbiol 12:249–263. https://doi.org/10.1186/1471-2180-12-249.
22. Singh K, Senadheera DB, Cvitkovitch DG. 2014. An intimate link: two-component signal transduction systems and metal transport systems in bacteria. Future Microbiol 9:1283–1293. https://doi.org/10.2217/fmb.14.87.
23. Bhagirath AY, Li Y, Patidar R, Yerex K, Ma X, Kumar A, Duan K. 2019. Two component regulatory systems and antibiotic resistance in Gram-negative pathogens. Int J Mol Sci 20:1781. https://doi.org/10.3390/ijms20071781.
24. Munson GP, Lam DL, Outten FW, O'Halloran TV. 2000. Identification of a copper-responsive two-component system on the chromosome of *Escherichia coli* K-12. J Bacteriol 182:5864–5871. https://doi.org/10.1128/jb.182.20.5864-5871.2000.
25. Gudipaty SA, Larsen AS, Rensing C, McEvoy MM. 2012. Regulation of Cu(I)/Ag(I) efflux genes in *Escherichia coli* by the sensor kinase CusS. FEMS Microbiol Lett 330:30–37. https://doi.org/10.1111/j.1574-6968.2012.02529.x.
26. Outten FW, Huffman DL, Hale JA, O'Halloran TV. 2001. The independent *cue* and *cus* systems confer copper tolerance during aerobic and anaerobic growth in *Escherichia coli*. J Biol Chem 276:30670–30677. https://doi.org/10.1074/jbc.M104122200.
27. Rouch DA, Brown NL. 1997. Copper-inducible transcriptional regulation at two promoters in the *Escherichia coli* copper resistance determinant *pco*. Microbiology 143:1191–1202. https://doi.org/10.1099/00221287-143-4-1191.
28. Grass G, Rensing C. 2001. Genes involved in copper homeostasis in *Escherichia coli*. J Bacteriol 183:2145–2147. https://doi.org/10.1128/JB.183.6.2145-2147.2001.
29. Zahid N, Zulfiqar S, Shakoori AR. 2012. Functional analysis of cus operon promoter of *Klebsiella pneumoniae* using *E. coli lacZ* assay. Gene 495:81–88. https://doi.org/10.1016/j.gene.2011.12.040.
30. Wu F, Ying Y, Yin M, Jiang Y, Wu C, Qian C, Chen Q, Shen K, Cheng C, Zhu L, Li K, Xu T, Bao Q, Lu J. 2019. Molecular characterization of a multidrug-resistant *Klebsiella pneumoniae* strain R46 Isolated from a rabbit. Int J Genomics 2019:5459190. https://doi.org/10.1155/2019/5459190.
31. Schelder S, Zaade D, Litsanov B, Bott M, Brocker M. 2011. The two-component signal transduction system CopRS of *Corynebacterium glutamicum* is required for adaptation to copper-excess stress. PLoS One 6:e22143. https://doi.org/10.1371/journal.pone.0022143.
32. Giner-Lamia J, López-Maury L, Reyes JC, Florencio FJ. 2012. The CopRS two-component system is responsible for resistance to copper in the cyanobacterium *Synechocystis sp. PCC 6803*. Plant Physiol 159:1806–1818. https://doi.org/10.1104/pp.112.200659.
33. Huertas MJ, López-Maury L, Giner-Lamia J, Sánchez-Riego AM, Florencio FJ. 2014. Metals in cyanobacteria: analysis of the copper, nickel, cobalt and arsenic homeostasis mechanisms. Life (Basel) 4:865–886. https://doi.org/10.3390/life4040865.
34. Mills SD, Jasalavich CA, Cooksey DA. 1993. A two-component regulatory system required for copper-inducible expression of the copper resistance operon of *Pseudomonas syringae*. J Bacteriol 175:1656–1664. https://doi.org/10.1128/jb.175.6.1656-1664.1993.
35. Mills SD, Lim CK, Cooksey DA. 1994. Purification and characterization of CopR, a transcriptional activator protein that binds to a conserved domain (cop box) in copper-inducible promoters of *Pseudomonas syringae*. Mol Gen Genet 244:341–351. https://doi.org/10.1007/BF00286685.
36. Zhang XX, Rainey PB. 2008. Regulation of copper homeostasis in *Pseudomonas fluorescens SBW25*. Environ Microbiol 10:3284–3294. https://doi.org/10.1111/j.1462-2920.2008.01720.x.
37. Hu YH, Wang HL, Zhang M, Sun L. 2009. Molecular analysis of the copper-responsive CopRSCD of a pathogenic *Pseudomonas fluorescens* strain. J Microbiol 47:277–286. https://doi.org/10.1007/s12275-008-0278-9.
38. Gao R, Stock AM. 2009. Biological insights from structures of two-component proteins. Annu Rev Microbiol 63:133–154. https://doi.org/10.1146/annurev.micro.091208.073214.
39. Desai SK, Kenney LJ. 2017. To ~P or not to ~P? Non-canonical activation by two-component response regulators. Mol Microbiol 103:203–213. https://doi.org/10.1111/mmi.13532.
40. Wolfe AJ. 2005. The acetate switch. Microbiol Mol Biol Rev 69:12–50. https://doi.org/10.1128/MMBR.69.1.12-50.2005.
41. Siryaporn A, Goulian M. 2008. Cross-talk suppression between the CpxA-CpxR and EnvZ-OmpR two-component systems in *E. coli*. Mol Microbiol 70:494–506. https://doi.org/10.1111/j.1365-2958.2008.06426.x.
42. Jacob-Dubuisson F, Mechaly A, Betton JM, Antoine R. 2018. Structural insights into the signalling mechanisms of two-component systems. Nat Rev Microbiol 16:585–593. https://doi.org/10.1038/s41579-018-0055-7.
43. Kenney LJ. 2010. How important is the phosphatase activity of sensor kinases? Curr Opin Microbiol 13:168–176. https://doi.org/10.1016/j.mib.2010.01.013.
44. Huffman DL, Huyett J, Outten FW, Doan PE, Finney LA, Hoffman BM, O'Halloran TV. 2002. Spectroscopy of Cu(II)-PcoC and the multicopper oxidase function of PcoA, two essential components of *Escherichia coli pco* copper resistance operon. Biochemistry 41:10046–10055. https://doi.org/10.1021/bi0259960.
45. Elsen S, Ragno M, Attree I. 2011. PtrA is a periplasmic protein involved in Cu tolerance in *Pseudomonas aeruginosa*. J Bacteriol 193:3376–3378. https://doi.org/10.1128/JB.00159-11.

Downloaded from http://msphere.asm.org/ on December 23, 2020 by guest

46. Ha UH, Kim J, Badrane H, Jia J, Baker HV, Wu D, Jin S. 2004. An in vivo inducible gene of *Pseudomonas aeruginosa* encodes an anti-ExsA to suppress the type III secretion system. Mol Microbiol 54:307–320. https://doi.org/10.1111/j.1365-2958.2004.04282.x.
47. Affandi T, Issaian AV, McEvoy MM. 2016. The structure of the periplasmic sensor domain of the histidine kinase CusS shows unusual metal ion coordination at the dimeric interface. Biochemistry 55:5296–5306. https://doi.org/10.1021/acs.biochem.6b00707.
48. Gudipaty SA, McEvoy MM. 2014. The histidine kinase CusS senses silver ions through direct binding by its sensor domain. Biochim Biophys Acta 1844:1656–1661. https://doi.org/10.1016/j.bbapap.2014.06.001.
49. Yoneyama H, Nakae T. 1996. Protein C (OprC) of the outer membrane of *Pseudomonas aeruginosa* is a copper-regulated channel protein. Microbiology 142:2137–2144. https://doi.org/10.1099/13500872-142-8-2137.
50. Huynh TN, Stewart V. 2011. Negative control in two-component signal transduction by transmitter phosphatase activity. Mol Microbiol 82:275–286. https://doi.org/10.1111/j.1365-2958.2011.07829.x.
51. Casino P, Rubio V, Marina A. 2009. Structural insight into partner specificity and phosphoryl transfer in two-component signal transduction. Cell 139:325–336. https://doi.org/10.1016/j.cell.2009.08.032.
52. Waldron KJ, Rutherford JC, Ford D, Robinson NJ. 2009. Metalloproteins and metal sensing. Nature 460:823–830. https://doi.org/10.1038/nature08300.
53. Reyes-Caballero H, Campanello GC, Giedroc DP. 2011. Metalloregulatory proteins: metal selectivity and allosteric switching. Biophys Chem 156:103–114. https://doi.org/10.1016/j.bpc.2011.03.010.
54. Xiao Z, Brose J, Schimo S, Ackland SM, La Fontaine S, Wedd AG. 2011. Unification of the copper(I) binding affinities of the metallo-chaperones Atx1, Atox1, and related proteins: detection probes and affinity standards. J Biol Chem 286:11047–11055. https://doi.org/10.1074/jbc.M110.213074.
55. Changela A, Chen K, Xue Y, Holschen J, Outten CE, O'Halloran TV, Mondragon A. 2003. Molecular basis of metal-ion selectivity and zeptomolar sensitivity by CueR. Science 301:1383–1387. https://doi.org/10.1126/science.1085950.
56. Raimunda D, Padilla-Benavides T, Vogt S, Boutigny S, Tomkinson KN, Finney LA, Argüello JM. 2013. Periplasmic response upon disruption of transmembrane Cu(+) transport in *Pseudomonas aeruginosa*. Metallomics 5:144–151. https://doi.org/10.1039/c2mt20191g.
57. Ekici S, Yang H, Koch HG, Daldal F. 2012. Novel transporter required for biogenesis of *cbb3*-type cytochrome *c* oxidase in *Rhodobacter capsulatus*. mBio 3:e00293-11. https://doi.org/10.1128/mBio.00293-11.
58. Teitzel GM, Geddie A, De Long SK, Kirisits MJ, Whiteley M, Parsek MR. 2006. Survival and growth in the presence of elevated copper: transcriptional profiling of copper-stressed *Pseudomonas aeruginosa*. J Bacteriol 188:7242–7256. https://doi.org/10.1128/JB.00837-06.
59. Quaranta D, McCarty R, Bandarian V, Rensing C. 2007. The copper-inducible cin operon encodes an unusual methionine-rich azurin-like protein and a pre-Q0 reductase in *Pseudomonas putida KT2440*. J Bacteriol 189:5361–5371. https://doi.org/10.1128/JB.00377-07.
60. Laub MT, Goulian M. 2007. Specificity in two-component signal transduction pathways. Annu Rev Genet 41:121–145. https://doi.org/10.1146/annurev.genet.41.042007.170548.
61. Capdevila DA, Edmonds KA, Giedroc DP. 2017. Metallochaperones and metalloregulation in bacteria. Essays Biochem 61:177–200. https://doi.org/10.1042/EBC20160076.
62. Rae TD, Schmidt PJ, Pufahl RA, Culotta VC, O'Halloran TV. 1999. Undetectable intracellular free copper: the requirement of a copper chaperone for superoxide dismutase. Science 284:805–808. https://doi.org/10.1126/science.284.5415.805.
63. Arts IS, Gennaris A, Collet JF. 2015. Reducing systems protecting the bacterial cell envelope from oxidative damage. FEBS Lett 589:1559–1568. https://doi.org/10.1016/j.febslet.2015.04.057.
64. Walker KW, Gilbert HF. 1994. Effect of redox environment on the *in vitro* and *in vivo* folding of RTEM-1 beta-lactamase and *Escherichia coli* alkaline phosphatase. J Biol Chem 269:28487–28493.
65. Huston WM, Jennings MP, McEwan AG. 2002. The multicopper oxidase of *Pseudomonas aeruginosa* is a ferroxidase with a central role in iron acquisition. Mol Microbiol 45:1741–1750. https://doi.org/10.1046/j.1365-2958.2002.03132.x.
66. Singh SK, Grass G, Rensing C, Montfort WR. 2004. Cuprous oxidase activity of CueO from *Escherichia coli*. J Bacteriol 186:7815–7817. https://doi.org/10.1128/JB.186.22.7815-7817.2004.
67. Argüello JM, Patel SJ, Quintana J. 2016. Bacterial Cu(+)-ATPases: models for molecular structure-function studies. Metallomics 8:906–914. https://doi.org/10.1039/c6mt00089d.
68. Thaden JT, Lory S, Gardner TS. 2010. Quorum-sensing regulation of a copper toxicity system in *Pseudomonas aeruginosa*. J Bacteriol 192:2557–2568. https://doi.org/10.1128/JB.01528-09.
69. Outten FW, Outten CE, Hale J, O'Halloran TV. 2000. Transcriptional activation of an *Escherichia coli* copper efflux regulon by the chromosomal MerR homologue, CueR. J Biol Chem 275:31024–31029. https://doi.org/10.1074/jbc.M006508200.
70. Drees SL, Beyer DF, Lenders-Lomscher C, Lubben M. 2015. Distinct functions of serial metal-binding domains in the *Escherichia coli* P1B -ATPase CopA. Mol Microbiol 97:423–438. https://doi.org/10.1111/mmi.13038.
71. Pezza A, Pontel LB, López C, Soncini FC. 2016. Compartment and signal-specific codependence in the transcriptional control of *Salmonella* periplasmic copper homeostasis. Proc Natl Acad Sci U S A 113:11573–11578. https://doi.org/10.1073/pnas.1603192113.
72. Held K, Ramage E, Jacobs M, Gallagher L, Manoil C. 2012. Sequence-verified two-allele transposon mutant library for Pseudomonas aeruginosa PAO1. J Bacteriol 194:6387–6389. https://doi.org/10.1128/JB.01479-12.
73. Jacobs MA, Alwood A, Thaipisuttikul I, Spencer D, Haugen E, Ernst S, Will O, Kaul R, Raymond C, Levy R, Chun-Rong L, Guenthner D, Bovee D, Olson MV, Manoil C. 2003. Comprehensive transposon mutant library of *Pseudomonas aeruginosa*. Proc Natl Acad Sci U S A 100:14339–14344. https://doi.org/10.1073/pnas.2036282100.
74. Choi KH, Schweizer HP. 2006. Mini-Tn7 insertion in bacteria with single attTn7 sites: example *Pseudomonas aeruginosa*. Nat Protoc 1:153–161. https://doi.org/10.1038/nprot.2006.24.
75. Gibson DG, Smith HO, Hutchison CA, III, Venter JC, Merryman C. 2010. Chemical synthesis of the mouse mitochondrial genome. Nat Methods 7:901–903. https://doi.org/10.1038/nmeth.1515.
76. Bradford MM. 1976. A rapid and sensitive method for the quantitation of microgram quantities of protein utilizing the principle of protein-dye binding. Anal Biochem 72:248–254. https://doi.org/10.1006/abio.1976.9999.
77. Bagchi P, Morgan MT, Bacsa J, Fahrni CJ. 2013. Robust affinity standards for Cu(I) biochemistry. J Am Chem Soc 135:18549–18559. https://doi.org/10.1021/ja408827d.
78. Xiao Z, Wedd AG. 2010. The challenges of determining metal-protein affinities. Nat Prod Rep 27:768–789. https://doi.org/10.1039/b906690j.
79. Crow JP, Sampson JB, Zhuang Y, Thompson JA, Beckman JS. 1997. Decreased zinc affinity of amyotrophic lateral sclerosis-associated superoxide dismutase mutants leads to enhanced catalysis of tyrosine nitration by peroxynitrite. J Neurochem 69:1936–1944. https://doi.org/10.1046/j.1471-4159.1997.69051936.x.
80. UniProt Consortium. 2019. UniProt: a worldwide hub of protein knowledge. Nucleic Acids Res 47:D506–D515. https://doi.org/10.1093/nar/gky1049.
81. Madeira F, Park YM, Lee J, Buso N, Gur T, Madhusoodanan N, Basutkar P, Tivey ARN, Potter SC, Finn RD, Lopez R. 2019. The EMBL-EBI search and sequence analysis tools APIs in 2019. Nucleic Acids Res 47:W636–W641. https://doi.org/10.1093/nar/gkz268.
82. Waterhouse AM, Procter JB, Martin DMA, Clamp M, Barton GJ. 2009. Jalview version 2—a multiple sequence alignment editor and analysis workbench. Bioinformatics 25:1189–1191. https://doi.org/10.1093/bioinformatics/btp033.
83. Waterhouse A, Bertoni M, Bienert S, Studer G, Tauriello G, Gumienny R, Heer FT, de Beer TAP, Rempfer C, Bordoli L, Lepore R, Schwede T. 2018. SWISS-MODEL: homology modelling of protein structures and complexes. Nucleic Acids Res 46:W296–W303. https://doi.org/10.1093/nar/gky427.
84. Pettersen EF, Goddard TD, Huang CC, Couch GS, Greenblatt DM, Meng EC, Ferrin TE. 2004. UCSF Chimera–a visualization system for exploratory research and analysis. J Comput Chem 25:1605–1612. https://doi.org/10.1002/jcc.20084.

Downloaded from http://msphere.asm.org/ on December 23, 2020 by guest

SUPPLEMENTAL MATERIAL LEGENDS

[Author: Because the full supplemental material legends will appear in the HTML version of the article online, and because the copy editor may have made changes, we have reproduced the legends below. Feel free to enter your changes on this page and we will see that they are conveyed to the online article.]

FIG S1 Topology, functional domains, and location of transposon insertions in CopS. The periplasmic Cu^+ sensor domain of CopS is highlighted (black solid line). His_{41} and His_{140} in blue and Phe_{42} in yellow are the residues forming the metal binding site. The C-terminal, cytoplasmic effector domain (black dotted line) contains the phosphorylatable His_{235} (red). Both insertional mutants, PW5705 and PW5706, have in-frame stop codons, producing shorter versions of CopS, lacking either part of the Cu binding residues and the effector domain (PW5705) or just the effector domain (PW5706). The CopS topology model was created using the Protter online tool version 1.0 (U. Omasits, C. H. Ahrens, S. Müller, and B. Wollscheid, Bioinformatics 30:884–886, 2014, https://doi.org/10.1093/bioinformatics/btt607).

FIG S2 Expression of genes in the CopRS regulon in the Δ*copR* and Δ*copS* mutant strains quantified in the absence (white) and the presence (black) of 0.5, 2, and 4 mM $CuSO_4$ (5-min treatment). Transcript levels of *pcoA*, *pcoB*, *PA2807*, *ptrA*, and *queF* genes are plotted relative to that of the housekeeping gene *PA4268*. Data are the mean ± SEM from three independent experiments.

FIG S3 Expression of the *copRS* operon in the Δ*copR* and Δ*copS* mutant strains quantified in the absence (white) and the presence (black) of 0.5, 2, and 4 mM $CuSO_4$ (5-min treatment). Transcript levels of *copR* and *copS* genes are plotted relative to that of the housekeeping gene *PA4268*. Data are the mean ± SEM from three independent experiments.

FIG S4 Expression of Cu transporter genes in the Δ*copR* and Δ*copS* mutant strains quantified in the absence (white) and the presence (black) of 0.5, 2, and 4 mM $CuSO_4$ (5-min treatment) (11). Transcript levels of *copA1*, coding for the Cu^+ efflux P_{1B}-type ATPase CopA1; *cusA*, a component of the RND CusABC system (A); and *oprC*, coding for Cu importer OprC (B), are plotted relative to that of the housekeeping gene *PA4268*. Data are the mean ± SEM from three independent experiments.

FIG S5 Cu tolerance of Δ*ackA* and Δ*pta* mutant strains. Growth rate of WT, Δ*copR*, Δ*copS*, Δ*ackA*, and Δ*pta* strains in the presence of 0 to 4 mM $CuSO_4$. Data are the mean ± SEM from at least three independent experiments.

FIG S6 Multiple sequence alignment of the *P. aeruginosa* CopRS TCS proteins with bacterial homologs. (A) *P. aeruginosa* CopR protein sequence was aligned with characterized bacterial RR to identify the conserved phosphorylatable Asp residue (highlighted in blue). (B) *P. aeruginosa* CopS and *E. coli* CusS protein sequences were

10/12/20 | 21:01 | ArtID: | DOI:10.1128/mSphere.01193-20 | CE: kmm

aligned with homologs of both of CopS-like and CusS-like proteins from different species. Conserved Cu binding sites at the dimeric interface are highlighted in yellow. *E. coli* CusS Cu binding sites, not conserved in CopS, are highlighted in orange. The conserved phosphorylatable His residue is highlighted in blue. UniProt accession numbers precede each species name.

FIG S7 SDS-PAGE analysis of the periplasmic copper binding loop of $CopS_{(34-151)}$. Ten micrograms of purified His_6-tagged (A) or Strep-tagged (B) protein was subjected to 8 to 16% gradient SDS-PAGE. Gels were stained with Coomassie blue G250. Left lanes: molecular weight marker. Right lanes: purified proteins. Arrows indicate the protein monomers and dimers, with expected masses of 19 and 38 kDa, respectively. The presence of the C-terminal His_6 tag in $CopS_{(34-151)}$ stabilized the dimer form of the protein. The C-terminal Strep tag did not. The gel shown in panel A was spliced for labeling purposes (blue vertical line).

FIG S8 Phylogenetic tree of CopS-like and CusS-like proteins. Separately, *P. aeruginosa* CopS and *E. coli* CusS were used to find homologs in the UniProtKB database. The top 20 hits (>45% homology) from each BLAST search were aligned with Clustal Omega, and the resulting alignment was used to construct the displayed average distance tree. Different taxa were colored as follows: dark blue, *Enterobacterales*; cyan, *Burkholderiales*; and pale violet, *Pseudomonadales*. UniProt accession numbers precede each species name.

TABLE S1 Bacterial strains, plasmids, and primers used in this study.

ID: mandar.gawadeTime: 21:01I Path: //mbnas01.cadmus.com/home$/sagar.dumbre$/SM-MSPH200025

Table S1. Bacterial strains, plasmids and primers used in this study

Strains	Relevant features	Reference
Pseudomonas aeruginosa		
PAO1	Wild type	(1)
Δ*copA1*	PW7626, *copA1*(PA3920)::ISphoA/hah::Tet^R	(2)
Δ*copR*	PW5704, *copR*(PA2809)::IslacZ/hah::Tet^R	(2)
copRcomp	Δ*copR* complemented with *copR* gene under endogenous promoter; C-term His_6; Gm^R	This study
$copR_{D51A}$	Δ*copR* complemented with $copR_{D51A}$ gene under endogenous promoter; C-term His_6; Gm^R	This study
$copR_{D51A}$	Δ*copR* complemented with $copR_{D51E}$ gene under endogenous promoter; C-term His_6; Gm^R	This study
Δ*copS*	PW5705, *copS*(PA2810)::IsphoA/hah::Tet^R	(2)
Δ*copS*	PW5706, *copS*(PA2810)::IsphoA/hah::Tet^R	(2)
copScomp	Δ*copS* complemented with *copS* gene under endogenous promoter; C-term His_6; Gm^R	This study
$copS_{H235A}$	Δ*copS* complemented with $copS_{H235A}$ gene under endogenous promoter; C-term His_6; Gm^R	This study
Escherichia coli		
Top10	*F^- mcrA Φ80lacZΔM15 ΔlacX74 recA1 araD139 Δ(ara-leu)7697 galU galK rpsL (Str^R) endA1 nupG*	Invitrogen
LMG194	*F- ΔlacX74 gal E thi rpsL ΔphoA (Pvu II) Δara714 leu::Tn10*	Invitrogen
SM10(λpir)/pTNS2	*thi-1, thr, leu, tonA, lacY, supE, recA::RP4-2- Tc::Mu, pir / pTNS2* (Amp^R *oriR6K, tnsABCDE*); Km^R/Helper plasmid (TnsABCD site), Amp^R	(3)
HB101/pRK2013	*F- mcrB mrr hsdS20(rB- mB-) recA13 leuB6 ara-14 proA2 lacY1 galK2 xyl-5 mtl-1 rpsL20 (Sm^R) glnV44 λ- / pRK2013* (Km^R *oriColE1 RK2-Mob+ RK2-Tra+*)	(3)
Plasmids	**Relevant features**	**Reference**
pBADtopo	*araBAD* promoter, V5 epitope tag, His_6-tag, Amp^R	Invitrogen
$CopS_{(34-151)}$_His_6:pBAD	DNA fragment encoding for the periplasmic copper binding loop of CopS residues 34 to 151. C-term His_6-tag, Amp^R	This study
$CopS_{(34-151)}$_Strep:pBAD	DNA fragment encoding for the periplasmic copper binding loop of CopS residues 34 to 151. C-term Strep-tag, Amp^R	This study
pUC18_mini_Tn7T_Gm	Suicide delivery vector, Tn7 transposable site, Gm^R	(4)
500prom_copR: pUC18_miniTn7T_Gm	500 bp upstream of *copR* gene + *copR* gene_His_6 cloned into the suicide delivery vector, Gm^R	This study
500prom_$copR_{D51A}$: pUC18_miniTn7T_Gm	500 bp upstream of *copR* gene + $copR_{D51A}$ gene_His_6 cloned into the suicide delivery vector, Gm^R	This study
500prom_$copR_{D51E}$: pUC18_miniTn7T_Gm	500 bp upstream of *copR* gene + $copR_{D51E}$ gene_His_6 cloned into the suicide delivery vector, Gm^R	This study
500prom_copS: pUC18_miniTn7T_Gm	500 bp upstream of *copR* gene + *copS* gene_His_6 cloned into the suicide delivery vector, Gm^R	This study
500prom_$copS_{H235A}$: pUC18_miniTn7T_Gm	500 bp upstream of *copR* gene + $copS_{H235A}$ gene_His_6 cloned into the suicide delivery vector, Gm^R	This study
Primers	**Sequence (5'-3')**	**Gene**
qPCR		
qPA4268_F	gcaaaactgcccgcaacgtc	housekeeping
qPA4268_R	tacacgaccgccacggatca	
qPA2064_F	aggtcaacctgtacggcagg	*pcoB*
qPA2064_R	aactcgcgacggatctcatagcg	

Primers	Sequence (5’-3’)	Gene
qPA2065_F	caagcacaccatcgacatgcc	*pcoA*
qPA2065_R	atgcgttgtctccttcgtctaccc	
qPA2806_F	ctgtttcccatttcacgcac	*queF*
qPA2806_R	gtagcagttccagatatccacg	
qPA2807_F	cgatggagattccccgta	*PA2807*
qPA2807_R	cgaggacgatcagggaag	
qPA2808_F	ggcgacatcgtcttcgag	*ptrA*
qPA2808_R	tccttcttcgtcgcttcg	
qPA2809_F	tgctcgaactgctgctgc	*copR*
qPA2809_R	acctcgatgacgttggtatcgc	
qPA2810_F	agatacgtatccgtctcggcgacc	*copS*
qPA2810_R	acgatagaaccggtcgaacaggc	
qPA3522_F	agtacaacagctggctgttgcc	*cusA*
qPA3522_R	tggacgaacacgttgttgtcgc	
qPA3920_R	gaaacggtgctggcgaagat	*copA1*
qPA3920_R	ttaaccagggcctgctccag	
qPA3790_F	gacggctcgcagttcaag	*oprC*
qPA3790_R	gctgacgttcgatttgacg	
Mutants complementation		
pUC_copR_His_F	aactgcagtgtcgggagcattacatc	
pUC_copR_His_R	ggactagttcaatggtgatggtgatgatgggactgaaaatacaggttttcgccgctgctttcgtcgcgctcttcgag	
copSR_promot_GA_F	catgagctcattttctgcagtgtcgggagcattacatc	
copS_prom_over_R	acatccgcgagccgaacccggcgctcatgttcatccctcgttacatt	
copS_whole_F	agcgccgggttcggctcg	
copS_pUC_His_GA_R	taccgggcccttttaagctttcaatgatgatgatgatgatgtcggcgcgggcgagcgaa	
pUCTn7Gm_GA_F	aagcttaaaagggcccggtacctcgcga	
pUCTn7Gm_GA_R	ctgcagaaaatgagctcatgcatgatcg	
Site mutants		
copS_H235A_F	gcagagttgcgcaccccgctcaccagc	
copS_H235A_R	agcggggtgcgcaactctgcggcgatgtcggcggagaac	
copR_D51A_F	gcagtcatgctgcccggccgtgac	
copR_D51A_R	cggccgggcagcatgactgcgaggatcagcaggtcgtagtcg	
copR_D51E_F	gaagtcatgctgcccggccgtgac	
copR_D51E_R	cggccgggcagcatgacttcgaggatcagcaggtcgtagtcg	
Protein expression		
copSsol_Strep_F	ttcagcagggccatcgac	
copSsol_Strep_R	tcatttttcgaactgcgggtggctccaagcgctcaactggcgcatgcgttg	
copSsol_TEV_His_R	ggactgaaaatacaggttttcgccgctgctcaactggcgcatgcgttg	

1. Winsor GL, Griffiths EJ, Lo R, Dhillon BK, Shay JA, Brinkman FS. 2015. Nucleic acids research 44:D646-D653.
2. Jacobs MA, Alwood A, Thaipisuttikul I, Spencer D, Haugen E, Ernst S, Will O, Kaul R, Raymond C, Levy R, Chun-Rong L, Guenthner D, Bovee D, Olson MV, Manoil C. 2003. Proc Nat Acad Sci USA 100:14339-44.
3. Choi KH, Schweizer HP. 2006. Nat Protoc 1:153-61.
4. Choi K-H, Gaynor JB, White KG, Lopez C, Bosio CM, Karkhoff-Schweizer RR, Schweizer HP. 2005. Nature Methods 2:443.

807 **Fig. S1**

808

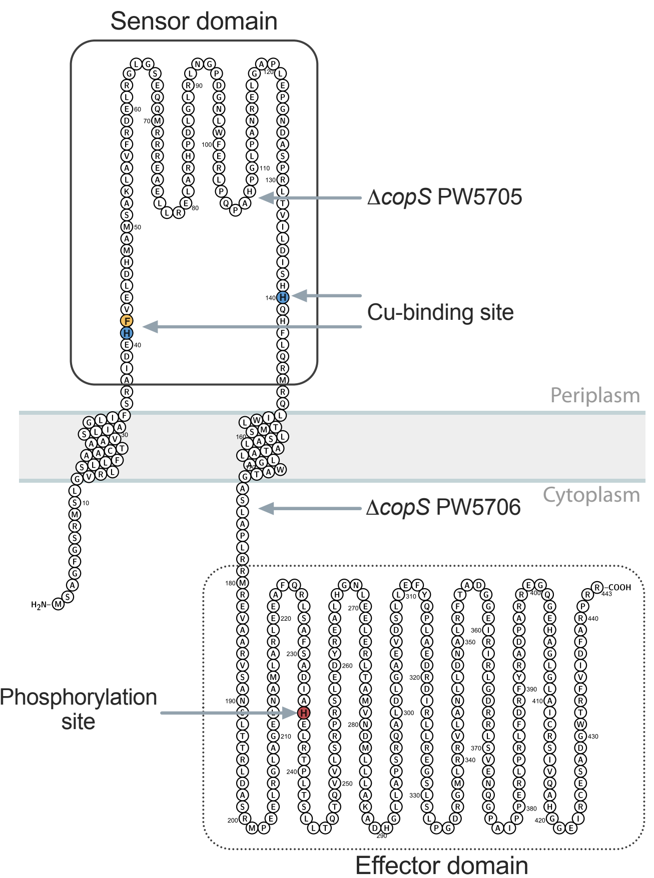

809

810

811 **Fig. S1.** Topology, functional domains, and location of transposon insertions in CopS.
812 The periplasmic Cu^{+} sensor domain of CopS is highlighted (black solid line). His_{41} and
813 His_{140} in blue, and Phe_{42}, in yellow are the residues forming the metal binding site. The
814 C-terminal, cytoplasmic effector domain (black dotted line), contains the phosphorylatable
815 His_{235} (red). Both insertional mutants, PW5705 and PW5706, have an in-frame stop
816 codons, producing shorter versions of CopS, lacking either part of the Cu-binding
817 residues and the effector domain (PW5705), or just the effector domain (PW5706). CopS
818 topology model was created using the Protter online tool version 1.0 (1).

819

820

821 1. Omasits U, Ahrens CH, Müller S, Wollscheid B. 2014. Bioinformatics 30:884-886.

822

823

824 **Fig. S2**
825
826

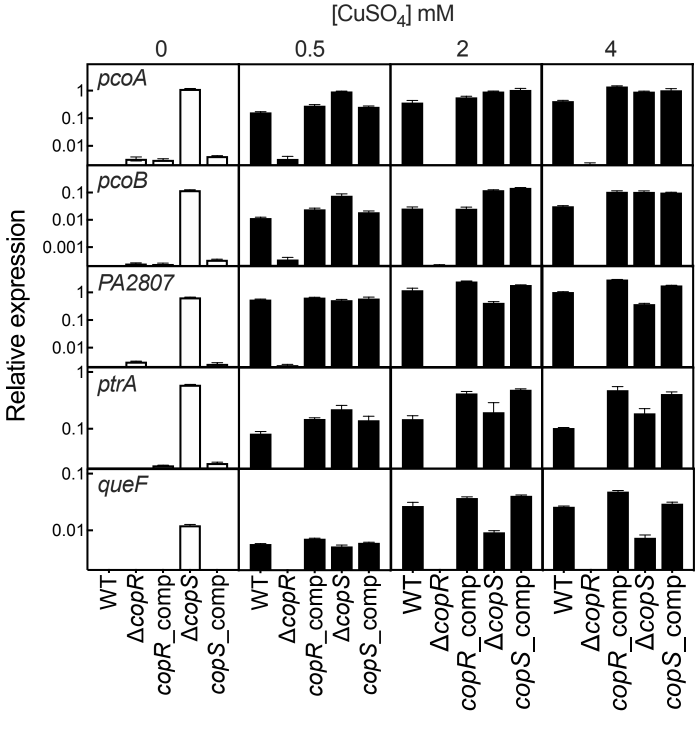

827
828
829
830 **Fig. S2.** Expression of genes in the CopRS regulon in the Δ*copR* and Δ*copS* mutant
831 strains quantified in the absence (white) and the presence (black) of 0.5, 2, and 4 mM
832 $CuSO_4$ (5 min treatment). Transcript levels of *pcoA*, *pcoB*, *PA2807*, *ptrA,* and *queF* genes
833 are plotted relative to that of the housekeeping gene *PA4268*. Data are the mean ± SEM
834 of three independent experiments.
835
836
837
838
839

840 **Fig. S3**
841
842

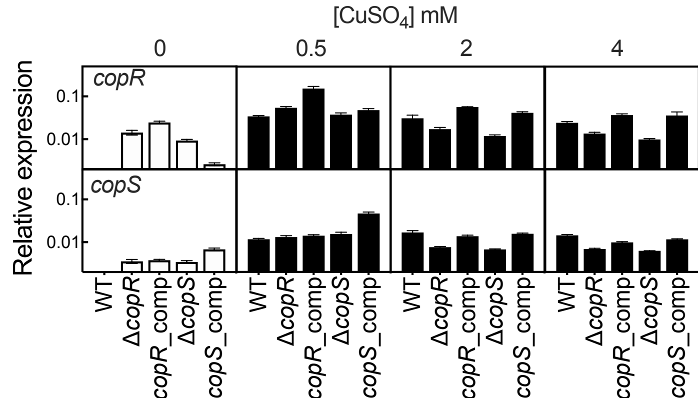

843
844
845
846 **Fig. S3.** Expression of the *copRS operon* in the Δ*copR* and Δ*copS* mutant strains
847 quantified in the absence (white) and the presence (black) of 0.5, 2, and 4 mM $CuSO_4$ (5
848 min treatment). Transcript levels of *copR*, and *copS* genes are plotted relative to that of
849 the housekeeping gene *PA4268*. Data are the mean ± SEM of three independent
850 experiments.
851
852
853

854 **Fig. S4**
855

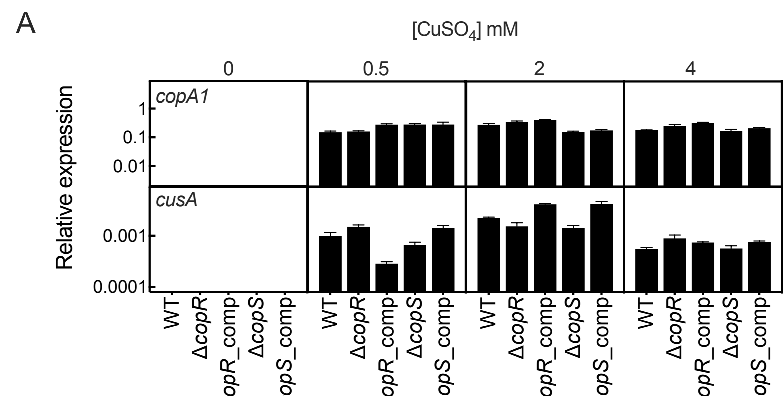

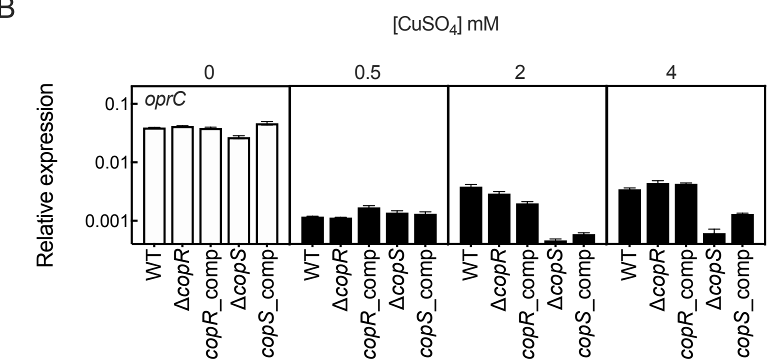

856
857
858
859 **Fig. S4.** Expression of Cu transporter genes in the Δ*copR* and Δ*copS* mutant strains
860 quantified in the absence (white) and the presence (black) of 0.5, 2 and 4 mM $CuSO_4$ (5
861 min treatment) (1). Transcript levels of *copA1,* coding for the Cu^+ efflux P_{1B}-type ATPase
862 CopA1, *cusA,* a component of the RND CusABC system (A), and *oprC,* codding for Cu
863 importer OprC (B), are plotted relative to that of the housekeeping gene *PA4268*. Data
864 are the mean ± SEM of three independent experiments.
865
866
867 1. Novoa-Aponte L, Ramírez D, Argüello JM. 2019. *J Biol Chem* 294:4934-4945.
868

869 **Fig. S5**
870
871

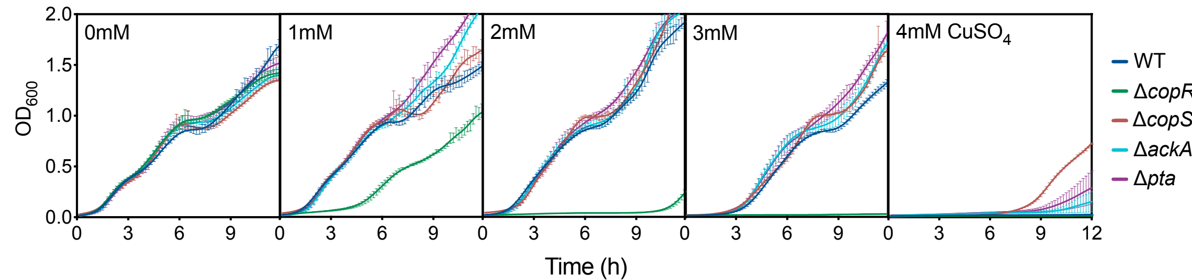

872
873
874
875 **Fig. S5.** Cu tolerance of Δ*ackA* and Δ*pta* mutant strains. Growth rate of WT, Δ*copR*,
876 Δ*copS*, Δ*ackA* and Δ*pta* strains in the presence of 0 - 4 mM $CuSO_4$. Data are the mean
877 ± SEM of at least three independent experiments.
878

Fig. S6

A

```
CopR_PA01                            ----MKLLIVEDEPRIGQYLRQGLAEAGFAVDLSDDGNEGEQLALGGDYDLLILDVMLPG   56
P0AA16_OmpR_Escherichia_coli         MQENYKILVVDDDMRLRALLERYLTEQGFQVRSVANAEQMDRLLTRESFHLMVLDLMLPG   60
P0AE88_CpxR_Escherichia_coli         ---MNKILLVDDDRELTSLLKELLEMEGFNVIVAHDGEQALDL-LDDSIDLLLLDVMMPK   56
P0AFJ5_PhoB_Escherichia_coli         --MARRILVVEDEAPIREMVCFVLEQNGFQPVEAEDYDSAVNQLNEPWPDLILLDWMLPG   58
P0DM78_PhoP_Salmonella_typhimurium   ---MMRVLVVEDNALLRHHLKVQLQDSGHQVDAAEDAREADYYLNEHLPDIAIVDLGLPD   57
                                          ::*:*:*:  :   :   *   *.      :  .          .: ::*  :*

CopR_PA01                            RDGWQILRSVRDAGM--TVPVLFLTARDAVEDRVRGLEQGADDYLVKPFAFVELLARVRT   114
P0AA16_OmpR_Escherichia_coli         EDGLSICRRLRSQSN--PMPIIMVTAKGEEVDRIVGLEIGADDYIPKPFNPRELLARIRA   118
P0AE88_CpxR_Escherichia_coli         KNGIDTLKALR-QTH--QTPVIMLTARGSELDRVLGLELGADDYLPKPFNDRELVARIRA   113
P0AFJ5_PhoB_Escherichia_coli         GSGIQFIKHLKRESMTRDIPVVMLTARGEEEDRVRGLETGADDYITKPFSPKELVARIKA   118
P0DM78_PhoP_Salmonella_typhimurium   EDGLSLIRRWRSSDV--SLPVLVLTAREGWQDKVEVLSSGADDYVTKPFHIEEVMARMQA   115
                                      .* .  :  :        *::.:**:    *::  *. *****: ***   *::**:::

CopR_PA01                            LLRRGSQQL-------QETTLQLADLELDLLRRRVQRQGKRIDLTAKEFALLELLLRRSG   167
P0AA16_OmpR_Escherichia_coli         VLRRQANELPGA-PSQEEAVIAFGKFKLNLGTREMFREDEPMPLTSGEFAVLKALVSHPR   177
P0AE88_CpxR_Escherichia_coli         ILRRSHWSEQQQNNDNGSPTLEVDALVLNPGRQEASFDGQTLELTGTEFTLLYLLAQHLG   173
P0AFJ5_PhoB_Escherichia_coli         VMRRISPMA-------VEEVIEMQGLSLDPTSHRVMAGEEPLEMGPTEFKLLHFFMTHPE   171
P0DM78_PhoP_Salmonella_typhimurium   LMRRNSG-L-------ASQVINIPPFQVDLSRRELSVNEEVIKLTAFEYTIMETLIRNNG   167
                                     ::**             . .: .  : ::   :.     : : :   *: ::  :  .

CopR_PA01                            EVLPKSLIASQVWDMNFDSDTNVIEVAIRRLRAKVDDD-YPQRLIHTVRGMGYVLEERDE   226
P0AA16_OmpR_Escherichia_coli         EPLSRDKLMNLARGREYSAMERSIDVQISRLRRMVEEDPAHPRYIQTVWGLGYVFVPDGS   237
P0AE88_CpxR_Escherichia_coli         QVVSREHLSQEVLGKRLTPFDRAIDMHISNLRRKLPDRKDGHPWFKTLRGRGYLMVSAS-   232
P0AFJ5_PhoB_Escherichia_coli         RVYSREQLLNHVWGTNVYVEDRTVDVHIRRLRKALEPG-GHDRMVQTVRGTGYRFSTRF-   229
P0DM78_PhoP_Salmonella_typhimurium   KVVSKDSLMLQLYPDAELRESHTIDVLMGRLRKKIQAQ-YPHDVITTVRGQGYLFELR--   224
```

B

```
CopS_PA01                          ---------------MSAGFGSRMSLGVRLSLLFAACTAAVSLIAGLIFSRAIDEHFVEL     45
Q88KY2_Pseudomonas_putida          -------------------MMRRVSLGSRLALLFAACTATVSLGAGLLFSRASEQHFVEL     41
C3K5G9_Pseudomonas_fluorescens     -------------------MIKRLSLASRLALLFAACTAVVSLIAGVLFNRASEAHFIEL     41
U3B9J6_Pseudomonas_alcaligenes     -----------------------MSLANRLALLFAACTAAVALLAGALFSRASEMHFIEL     37
A0A085VDP0_Pseudomonas_syringae    -------------------MIRRWSLASRLALLFAACTAVVSLIAGVLFNQASETHFIEL     41
CusS_E.coli                        --------------MVSKPFQRPFSLATRLTFFISLATIAAFFAFAWIMIHSVKVHFAEQ     46
Q83M20_Shigella_flexneri           --------------MVSKPFQRPFSLATRLTFFISLATIAAFFAFAWIIIHSVKVHFAEQ     46
A8AJR2_Citrobacter_koseri          --------------MVTKRFQRPFSLATRLTFFISLATIASFFAFAWIMIHSVKVHFAEQ     46
A0A378C5Z1_Klebsiella_pneumoniae   -----------------MAAKRPFSLATRLTFFISLATIIAFFAFTWIMIHSVKAHFEER     43
A0A4V2W4T5_Biostraticola_tofi      MPVSRSHRSFPRGIRSFLLATRPLSLAMRLTCFISLATIAAFVAFAWIMLHSVEHHFAEQ     60
                                                           **. **: ::: .*    .    :: :: . ** *

CopS_PA01                          DHMAMSAKLAVFRDELRGLGSEQQMRRREAELLRELARHPDLGLRLNGPDGNLWFERLPQ     105
Q88KY2_Pseudomonas_putida          DQQLLDSRLSLFRTQLAGVSTADELQARLPALRDELSHQADLALRISASNGATWFESRSG     101
C3K5G9_Pseudomonas_fluorescens     DQQQLDSQLVALRSTLQGVDSPELFAQREAQLRAELNRQPELALRITAQGQ-RWFDGAPG     100
U3B9J6_Pseudomonas_alcaligenes     DQQQLQGKLAVFTELLQGVTSTTALVARRPALEQELQRHPELALRIEGPDGQVWFSSRAL     97
A0A085VDP0_Pseudomonas_syringae    DQQLLESKLPGLRSLLQNVRSEQDLAGRAAQLKAELAHQPDLGLRISGPGSEPWFDSAAL     101
CusS_E.coli                        DINDLKEISATLERVLNHPDETQ--ARRLMTLEDIVSGYSNVLISLADSQGKTVYHSPGA     104
Q83M20_Shigella_flexneri           DINDLKEISATLERVLNHPDETQ--ARRLMTLEDIVSGYSNVLISLADSHGKTVYHSPGA     104
A8AJR2_Citrobacter_koseri          DINDLKEISATLERILTHPDEPE--ARRLEILKNVAAGYSNVIISLEDANQRAIFHSPGS     104
A0A378C5Z1_Klebsiella_pneumoniae   DVHDLRQLSTTLETVLDHADYPP--ARRLEIVRNIIAGYANVFICLDDGQGNILFQSPNG     101
A0A4V2W4T5_Biostraticola_tofi      DVSDLKQISATLANTLKKANEPQ--AEKVEKLRTALAGYRNIAVLLKTEDNRLLYRSADG     118
                                   *   :      :  *           :  :        :: : :        :

CopS_PA01                          PAHP---------------------------GL-------PANRELGAPLEPGNDA-SP     129
Q88KY2_Pseudomonas_putida          LPHA-----------------------AQATGLATLHAPGIDYRSLSVPLTQGAMQ-SP     136
C3K5G9_Pseudomonas_fluorescens     V--N----------------------LPTGPGLHSLQNAGTDYRVYNTPLRANQPD-SP     134
U3B9J6_Pseudomonas_alcaligenes     PDSL----------------------PHTQ----HWNHQDTAYRVMSTK-----QG-DL     124
A0A085VDP0_Pseudomonas_syringae    KPSL----------------------PVTDEGLHTLISDQTAYRTYTVKLDPATPD-SP     137
CusS_E.coli                        PDIREFTRDAIPDKDAQGGEVYLLSGPTMMMPGHGHGHMEHSNWRMINLPVGPLVDG-KP     163
Q83M20_Shigella_flexneri           PDIREFARDAIPDKDARGGEVYLLSGPTIMMPGHGHGHMEHSNWRMINLPVGPLVDG-KP     163
A8AJR2_Citrobacter_koseri          PDLRQFIAKATPDSSARNGDVFLLSSPDLQSKRHANGHGTHSAWRMIRLPVGQLADG-QP     163
A0A378C5Z1_Klebsiella_pneumoniae   PDLSHILSTPGLAMQLRDGNVISWTDPQPRAMAHDNHPMETRAWRLIMLPLGKQADG-KP     160
A0A4V2W4T5_Biostraticola_tofi      PDLDAIGSSPAFAANLASREVFTWSDTQSTQSAHGDS-AKHPAYRVIASTVQTRVAGKVT     177
                                                                          *

CopS_PA01                          RL--TVILDISHHQHFLQRMRQLIWLTMSLSALATALLGAWATGASLAPLRRMREVAARV     187
Q88KY2_Pseudomonas_putida          RL--TLYLDITHHQHFLQGMQRLIWLTVGLSALITALLGAWAARSGLRPLRQMGQVAASV     194
C3K5G9_Pseudomonas_fluorescens     QL--TLVLDITHHQHFLQRMQHLIWLTVGLSALATALLGAWAARSGLRPLRRMGEVAASV     192
U3B9J6_Pseudomonas_alcaligenes     RL--TLLLDITHHQHFLEQMQRLIWLCVGLSALATALLGAWVARRGLRPLRQMTRVTQQV     182
A0A085VDP0_Pseudomonas_syringae    QL--TLLLDITHHQHFLQRMQRLIWLTVGLSALATALLGAWAARSGLRPLHNMSRIAASV     195
CusS_E.coli                        IYTLYIALSIDFHLHYINDLMNKLIMTASVISILIVFIVLLAVHKGHAPIRSVSRQIQNI     223
Q83M20_Shigella_flexneri           IYTLYIALSIDFHLHYINDLMNKLIMTASVISILIVFIVLLAVHKGHAPIRSVSRQIQNI     223
A8AJR2_Citrobacter_koseri          AYTLYMALSIDFHLHYINDLKNKLIMTASLISMMIIFIVLFAVYKGHEPIRSVSRRIQNI     223
A0A378C5Z1_Klebsiella_pneumoniae   AYHLLMALSIDFHLHYINELKAKLISAASIISLLIIAIVLFVVYQGHKPIRQISRQIQNI     220
A0A4V2W4T5_Biostraticola_tofi      RYSLMIALSIDFHLHYIEELKHNLIMIAAGISLLIVFIVLFAVYKGHTPLRNVSKKIKNI     237
                                        : *.* .* *::: :   :     .  ::    :    ..  .  *:: : .    :

CopS_PA01                          SANSLTTRLDASRMPEELRGLAGELNAMLARLEEAFQRLSAFSADIAHELRTPLTSLLTQ     247
Q88KY2_Pseudomonas_putida          SARSLTTRLPVAQMPEELAELASSMNAMLQRLDDAFQRLSAFSADIAHELRTPLSNLLTH     254
C3K5G9_Pseudomonas_fluorescens     SAHSLTQRLPQQHMPVELAELAQTFNAMLSRLDDAFQRLSAFSADIAHELRTPLSNLLTQ     252
U3B9J6_Pseudomonas_alcaligenes     SASSLTARLPADALPAELGELAASFNAMLARLEDAFARLSAFSADIAHELRTPLSNLLTQ     242
A0A085VDP0_Pseudomonas_syringae    SASSLTTRLPQEQMPAELAELTQAFNGMLGRLDDGFQRLSAFSADIAHELRTPLSNLLTH     255
CusS_E.coli                        TSKDLDVRLDPQTVPIELEQLVLSFNHMIERIEDVFTRQSNFSADIAHEIRTPITNLITQ     283
Q83M20_Shigella_flexneri           TSKDLDVRLDPQTVPIELEQLVLSFNHMIERIEDVFTRQSNFSADIAHEIRTPITNLITQ     283
A8AJR2_Citrobacter_koseri          TSKDLDVRLDPQAVPIELERLVLSFNHMLERIEDVFTRQSNFSADIAHEIRTPITNLVTQ     283
A0A378C5Z1_Klebsiella_pneumoniae   TSRDLDVRLDPQAVPVELERLALSFNHMLERIEDVFTRQSNFSADIAHEIRTPITNLVTQ     280
A0A4V2W4T5_Biostraticola_tofi      TSENLDVRLDPHKVPIELEQLVISFNNMIERIEDVFTRQANFSADIAHEIRTPITNLITQ     297
                                   :: .*  **    :* **  *.  :* *: *::: * * : ********:***::.*:*:

CopS_PA01                          TQVVLSRPRSLEDYREALHGNLEELERLTAMVNDMLLLAKADHGLLAPSRQALDLGAEVD     307
Q88KY2_Pseudomonas_putida          TQVTLTRPRSLEEYREALHGNLEELQWMAQMINDMLFLAKADHGLLVPGDAPLALHDEVD     314
C3K5G9_Pseudomonas_fluorescens     TQVILTQPRPLEDYREALHSNLEELQWMAQLVNDMLYLAKADHGLLVPKREPLALADEVE     312
U3B9J6_Pseudomonas_alcaligenes     TQVILSQPRALEDYQEALHSNLEELQHLAQMVGDMLLLAKADNGLLQTRRETLALERELT     302
A0A085VDP0_Pseudomonas_syringae    TQVTLTRPRDIEDYREALLSNLEELQSMAQMVNDMLYLAKAEHGLLTPTCERLRLEDEVQ     315
CusS_E.coli                        TEIALSQSRSQKELEDVLYSNLEELTRMAKMVSDMLFLAQADNNQLIPEKKMLNLADEVG     343
Q83M20_Shigella_flexneri           TEIALSQSRSQKELEDVLYSNLEELTRMAKMVSDMLFLAQADNNQLIPEKKMLNLADEVG     343
A8AJR2_Citrobacter_koseri          TEIALSQTRSQKELEDVLYSNLEEFGRMSKMVSDMLFLAQADNNQLIPEKKALDLADEVH     343
A0A378C5Z1_Klebsiella_pneumoniae   TEIALSQSRSQQELEEVLYSNLEEFSRMSRMVSDMLFLAQADNNQLIPEQQALDLADEVH     340
A0A4V2W4T5_Biostraticola_tofi      TEIVLRQPRTIKELEDVLYSNLEEFSHMAKMVSDMLFLAQADNQQLIPERSLIDLETEVR     357
                                   *:: * : *  :: .:.* .****:  :: ::.*** **:*::  *       : *  *:
```

884

```
CopS_PA01                         SLLEFYQPLAEDRDIRLLREGSL-SLPGDRGMLRRVLANLLDNALRFTADGGEIRIRLGD     366
Q88KY2_Pseudomonas_putida         ALLEYYAPLAEDSDVQMLREGEA-VLHGDQHMLRRALSNLLDNAMRFTPAGGQIKVTLGP     373
C3K5G9_Pseudomonas_fluorescens    ALLEFFALLAEDAHVSLVREGTA-HTMGDRGMLRRALSNLLDNALRFTPAGGEVRVRMVD     371
U3B9J6_Pseudomonas_alcaligenes    ALAEYFTPLAEEAGVHLHVDGQA-ALSADRALLHRALSNLIDNALRFTPRGGELHLSSAQ     361
A0A085VDP0_Pseudomonas_syringae   TVLEFFAPLAEDAQVTLSSDGHA-SIDGDRTMLRRVLSNLLDNAVRHTPAGGYVKVTLSE     374
CusS_E.coli                       KVFDFFEALAEDRGVELRFVGDKCQVAGDPLMLRRALSNLLSNALRYTPTGETIVVRCQT     403
Q83M20_Shigella_flexneri          KVFDFFEALAEDRGVELRFVGDKRQVAGDPLMLRRALSNLLSNALRYTPTRETIVVRCQT     403
A8AJR2_Citrobacter_koseri         KVFDFFEAWAEEREVRLHFEGRACWVSGDPIMLRRALSNLLSNAMRYTPKGEAVTVRLKE     403
A0A378C5Z1_Klebsiella_pneumoniae  KVFEFFEAWAEEKAVALRFVGSHCRVIGDPLMLRRAISNLLSNAIRYTPAGQAVTIQLSE     400
A0A4V2W4T5_Biostraticola_tofi     KVFEFFEAWADEREVRLNITGRAQPIEGDPLMLRRAISNLLSNAVRYTPPGNTIIVQLTE     417
                                   : :::   *::  : :   *      .*  :*:*.::**:.**:*.*     : :

CopS_PA01                         ----RRLSVENQGPAIPPERLPRLFDRFYRADPARREGQGEHAGLGLAICRSIVQAHGGE     422
Q88KY2_Pseudomonas_putida         ---GPTINVANTGLAIDPAALPRLFDRFYRVDPARREGSSEHAGLGLAITRSIVQAHGGC     430
C3K5G9_Pseudomonas_fluorescens    ---GVTLTVENTGAGIPAQLLPRLFDRFYRADPARHEGSSEHAGLGLAITQSIVRAHGGR     428
U3B9J6_Pseudomonas_alcaligenes    QGAKVRIEVANQGPEIPLDLRERLFDRFYRADPARREGGAEHAGLGLAIARSIVQAHGGA     421
A0A085VDP0_Pseudomonas_syringae   VDKRARINVENSGADIPESLLPRLFDRFYRADQARSE-SREHAGLGLAITRSIIQAHGGT     433
CusS_E.coli                       VDHLVQVIVENPGTPIAPEHLPRLFDRFYRVDPSRQR-KGEGSGIGLAIVKSIVVAHKGT     462
Q83M20_Shigella_flexneri          VDHQVQVSVENPGTPIAPEHLPRLFDRFYRVDPSRQR-KGEGSGIGLAIVKSIVVAHKGT     462
A8AJR2_Citrobacter_koseri         MDRQAQITVENPGAPIAPEHLPRLFDRFYRVDPSRQR-KGEGSGIGLAIVKSIVIAHQGT     462
A0A378C5Z1_Klebsiella_pneumoniae  SAETVRLVVENPGTPIAAEHLPRLFDRFYRVDPSRQR-KGEGSGIGLAIVKSIVGAHHGS     459
A0A4V2W4T5_Biostraticola_tofi     RDQWVEIQVENPGAMIAEQHLPRLFDRFYRADPSRQK-KGEGSGIGLAIVKSIVTAHQGK     476
                                        : * * *  *      ********.* :* .   * :*:**** :**: ** *

CopS_PA01                         IRCESADGWTRFVIDFARPRR  443
Q88KY2_Pseudomonas_putida         IRAECEGGWTRFVIEFTQDR-  450
C3K5G9_Pseudomonas_fluorescens    IYCESGAGWTRFVIELPAGD-  448
U3B9J6_Pseudomonas_alcaligenes    IRCESAEGWTRFILEFPA---  439
A0A085VDP0_Pseudomonas_syringae   IRCESKEGVTRFLIELPIQK-  453
CusS_E.coli                       VAVTSDARGTRFVITLPA---  480
Q83M20_Shigella_flexneri          VAVTSDARGTRFVITLPA---  480
A8AJR2_Citrobacter_koseri         VSVTSDLRATRFILTLPKHGD  483
A0A378C5Z1_Klebsiella_pneumoniae  VAAQSDLRSTRFIVVLPK---  477
A0A4V2W4T5_Biostraticola_tofi     ISVSSDAVSTKFSLSLPKRAS  497
                                  :   .   *:* : :
```

885
886
887
888
889
890
891
892
893
894
895

Fig. S6. Multiple sequence alignment of the *P. aeruginosa* CopRS TCS proteins with bacterial homologs. (A) *P. aeruginosa* CopR protein sequence was aligned with characterized bacterial RR to identify the conserved phosphorylatable Asp residue (highlighted in blue). (B) *P. aeruginosa* CopS and *E. coli* CusS protein sequences were aligned with homologs of both of CopS-like and CusS-like proteins from different species. Conserved Cu binding sites at the dimeric interface are highlighted in yellow. *E. coli* CusS Cu binding sites, not conserved in CopS, are highlighted in orange. The conserved phosphorylatable His residue is highlighted in blue. Uniprot accession numbers precede each species name.

896
897
898
899

900 **Fig. S7**

901
902

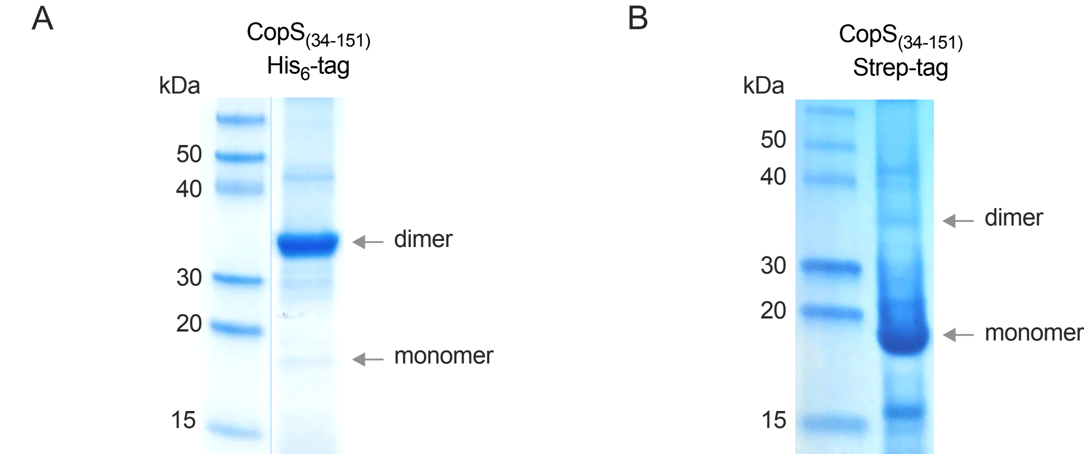

903
904
905
906 **Fig. S7.** SDS-PAGE analysis of the periplasmic copper binding loop of $CopS_{(34-151)}$. 10
907 μg of purified (A) His_6-tagged or (B) strep-tagged protein were subjected to 8-to-16%
908 gradient SDS-PAGE. Gels were stained with Coomassie Blue G250. Left lanes: molecular
909 weight marker. Right lanes: purified proteins. Arrows indicate the protein monomers and
910 dimers, with expected masses of 19 and 38 kDa, respectively. The presence of the C-
911 terminal His_6-tag in $CopS_{(34-151)}$ stabilized the dimer form of the protein. The C-terminal
912 Strep-tag did not. The gel shown in (A) was spliced for labeling purposes (blue vertical
913 line).
914
915
916
917
918
919
920

921 **Fig. S8**

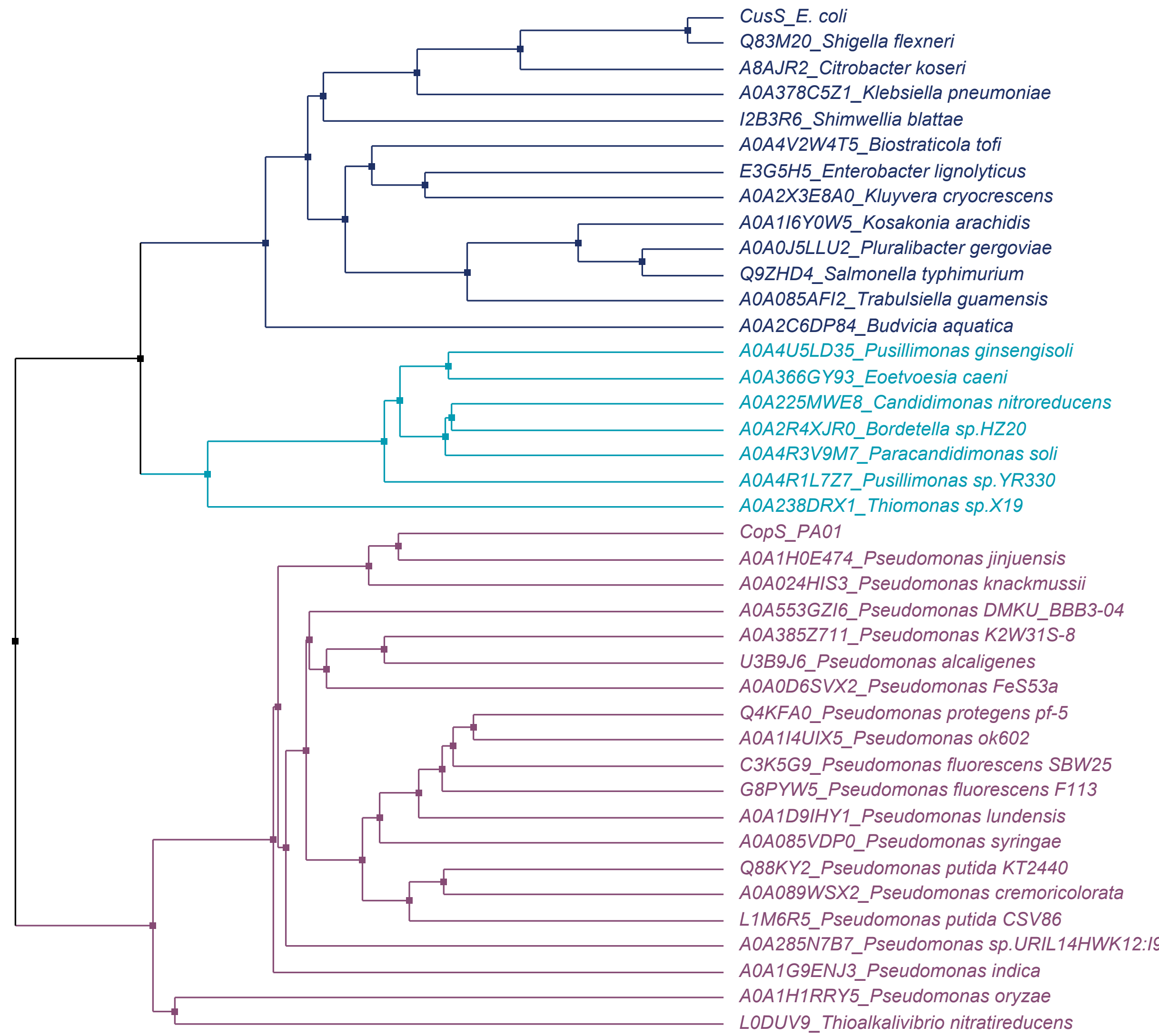

922
923
924
925 **Fig. S8.** Phylogenetic tree of CopS-like and CusS-like proteins. Separately, *P. aeruginosa*
926 CopS and *E. coli* CusS were used to find homologs in the UniProtKB database. The top-
927 20 hits (>45% homology) from each Blast search were aligned with Clustal Omega, and
928 the resulting alignment used to construct the displayed average distance tree. Different
929 taxa were colored as follow: dark blue, Enterobacterales; cyan, Burkholderiales; and
930 paleviolet, Pseudomonadales. Uniprot accession numbers precede each species name.

931